AERODYNAMIC EFFECTS OF NEARLY UNIFORM SLIPSTREAMS ON THIN WINGS IN THE TRANSONIC REGIME

By

Magdi H. Rizk

May 1980

Prepared Under Contract No. NAS2-9913

For

National Aeronautics and Space Administration

Ames Research Center
Moffett Field, California

By

Flow Research Company
A Division of Flow Industries, Inc.
Kent, Washington 98031

1. Report No.	2. Government Accession No.	3. Recipient's Catalog No.
NASA CR-152351		

4. Title and Subtitle	5. Report Date
Aerodynamic Effects of Nearly Uniform Slipstreams on Thin Wings in the Transonic Regime	May 1980
	6. Performing Organization Code

7. Author(s)	8. Performing Organization Report No.
M. H. Rizk	160
	10. Work Unit No.

9. Performing Organization Name and Address	11. Contract or Grant No.
Flow Research Company A Division of Flow Industries, Inc. 21414-68th Avenue South, Kent WA 98031	NAS2-9913
	13. Type of Report and Period Covered
12. Sponsoring Agency Name and Address	Final Report
National Aeronautics and Space Administration Ames Research Center Moffett Field CA 94035	14. Sponsoring Agency Code

15. Supplementary Notes

Technical Monitor: Daniel P. Bencze
NASA Ames Research Center
Moffett Field CA 94035

16 Abstract

An inviscid model for the interaction between a thin wing and a nearly uniform propeller slipstream is presented. The model allows the perturbation velocities due to the interaction to be potential, although the undisturbed slipstream velocity is rotational. A finite difference scheme is used to solve the governing equation. Numerical examples for a rectangular wing and a swept wing are presented. They indicate that the slipstream has a strong effect on the aerodynamic properties of the wing section within the slipstream and lesser effects elsewhere. The slipstream's swirling motion strongly affects the wing load distribution; however, its effect on the wing's total lift and wave drag is small. The axial velocity increment in the slipstream has a small effect on the wing lift; however, it causes a large increase in wave drag.

17. Key Words (Suggested by Author(s))	18. Distribution Statement
slipstream swirl potential flow	Unlimited Distribution

19. Security Classif. (of this report)	20. Security Classif. (of this page)	21. No. of Pages	22. Price*
Unclassified	Unclassified	53	

*For sale by the National Technical Information Service, Springfield, Virginia 22161

Table of Contents

Nomenclature

Symbol	Definition
a	speed of sound/$\hat{Q}_{o\infty}$
c	wing chord
c_ℓ	section lift coefficient
C_{mac}	wing mean aerodynamic chord
C_p	pressure coefficient
h	enthalpy/$\hat{Q}^2_{o\infty}$
i	computational mesh index in the z direction
I	maximum value of $i-1$
j	computational mesh index in the r direction
J	maximum value of $j-1$
k	computational mesh index in the ϕ direction
K	maximum value of k in the first quadrant
k_w	index of mesh plane in the first quadrant, neighboring the plane $\theta = \frac{\pi}{2}$
k_w'	index of mesh plane in the third quadrant, neighboring the plane $\theta = \frac{3\pi}{2}$
M	Mach number
p	pressure/$\hat{\rho}_{o\infty}\ \hat{Q}^2_{o\infty}$
$\underset{\sim}{q}$	perturbation velocity vector/$\hat{Q}_{o\infty}$
$\underset{\sim}{Q}$	velocity vector/$\hat{Q}_{o\infty}$
Q	flow speed/$\hat{Q}_{o\infty}$
$\hat{Q}$	flow speed
r	radial coordinate/c
R	radial coordinate of slipstream boundary/c
u	perturbation velocity component in the z direction/$\hat{Q}_{o\infty}$
U	velocity component in the z direction/$\hat{Q}_{o\infty}$
ΔU	deviation of U from its average value/$\hat{Q}_{o\infty}$
v	perturbation velocity component in the r direction/$\hat{Q}_{o\infty}$
V	velocity component in the r direction/$\hat{Q}_{o\infty}$
w	perturbation velocity component in the θ direction/$\hat{Q}_{o\infty}$
W	velocity component in the θ direction/$\hat{Q}_{o\infty}$
z	axial coordinate/c

Nomenclature (Cont.)

Symbol	Definition
α_s	slipstream swirl angle
γ	ratio of specific heats
$\underset{\sim}{\zeta}$	vorticity vector/$(\hat{Q}_{o\infty}/c)$
η	deviation of slipstream boundary from its undisturbed position/c
η^*	% of semispan
θ	angular coordinate
μ	$= \max\left[0, \left(1 - \frac{a^2}{Q^2}\right)\right]$
ξ_r	stretching factor in r direction
ξ_z	stretching factor in z direction
ξ_θ	stretching factor in θ direction
ρ	density/$\hat{\rho}_{o\infty}$
$\hat{\rho}$	density
ϕ	perturbation velocity potential/$c\hat{Q}_{o\infty}$
ψ	undisturbed radius of a streamline/$c\hat{Q}_{o\infty}$
Subscripts	
i	denotes inner region variables
o	denotes outer region variables
s	slipstream boundary
t	denotes total conditions
∞	denotes undisturbed conditions
Superscripts	
$\bar{(\ )}$	average quantity

1. Introduction

Interest in turbo-prop propulsion systems has been recently revived due to the propulsion efficiency of these systems and the predicted fuel shortages in the future. Propeller slipstreams will interact with wings causing changes in their aerodynamic properties. The determination of the effects of slipstream-wing interaction is therefore necessary before any design decisions regarding the installation of turbo-prop propulsion systems can be derived. Since current passenger flight cruise speeds are in the transonic range, this is the range considered here.

The interaction of wings with regions of high energy flow embedded in uniform streams was studied by Shollenberger (1975), who used flow singularities to simulate a jet interacting with a wing. The flow solution and jet position were found by calculating the singularity strengths and locations. Lan (1975) used a quasi vortex-lattice method and a two-vortex-sheet representation of the slipstream to study the interaction problem with different slipstream and freestream Mach numbers. Ting, et al., (1972) used the method of asymptotic expansions to study the interference of a wing with multipropellers. The effect of nonuniform streams on the aerodynamic characteristics of wings has been studied by Chow, et al., (1970) and Kleinstein and Liu (1972). Boctor, et al., (1978) have recently studied the interaction of the slipstream with a wing-body configuration at high subsonic Mach numbers, using the panel method. This method does not include treatment of local patches of supersonic flow and shock waves. Therefore, though it may indicate qualitative trends, it fails to give quantitative descriptions of flows in the transonic regime. In addition to the theoretical studies mentioned above, experimental tests were conducted by Welge and Crowder (1978) to assess the magnitude of the aerodynamic interference of a propeller slipstream on a supercritical wing.

Except for the final experimental study, all previous studies dealing with slipstream-wing interaction are limited to subsonic flows. In this report a simplified model is used to describe the interaction between a propeller slipstream and a wing in the transonic regime. The undisturbed slipstream boundary is assumed to coincide with an infinite

circular cylinder. The undisturbed slipstream velocity is rotational and is a function of the radius only. In general, the velocity perturbation caused by introducing a wing into the slipstream is also rotational. By making small disturbance assumptions, however, the perturbation velocity becomes nearly potential, and an approximation for the flow is obtained by solving a potential equation. This simplified model allows us to obtain basic information about the interaction problem while avoiding the need for solving the more complex Euler equations.

2. Formulation and Governing Equations

The present analysis considers a wing in a flow with a slipstream (inner flow region) embeaded in a freestream (outer flow region). Far upstream of the wing, flow conditions are undisturbed by the wing. There, the freestream Mach number is $M_{o\infty}$, and the slipstream is a circular cylinder of radius R_∞ with velocity distribution $\underset{\sim}{Q}_{i\infty} = (U_{i\infty}(r)\ ,\ 0\ ,\ W_{i\infty}(r))$ and total enthalpy $h_{ti\infty}(r)$. The flow velocities and the enthalpy are normalized here by the freestream flow speed and the square of the freestream flow speed, respectively. The cylindrical coordinates $(z,\ r,\ \theta)$ are used, with the z-axis coinciding with the axis of the undisturbed slipstream. The coordinates r and z are normalized by the wing chord. The subscripts i, o, ∞, and t are used

used to denote inner region properties, outer region properties, undisturbed conditions, and total conditions, respectively. As the wing is approached, the flow is perturbed from its basic undisturbed condition. Since the flow is potential in the outer flow region, the velocity perturbation there may be expressed as $\underset{\sim}{q}_o = \nabla\phi_o$. In the slipstream, the flow is rotational in general. Let $\underset{\sim}{q}_i = (u_i\ ,\ v_i\ ,\ w_i)$ be the velocity perturbation there. Due to the wing effect, the slipstream surface deviates from the undisturbed circular cylinder and is defined by

$$r = R(z,\theta) = R_\infty + \eta(z,\theta)\ ,$$

where η is the amount of deviation from the undisturbed condition.

The conditions at the interface specifying zero normal flow to it are

$$v_i = U_i\eta_z + W_i\frac{\eta_\theta}{R}\ ,\ r = R\ , \tag{1}$$

and

$$\phi_{o_r} = U_o\eta_z + W_o\frac{\eta_\theta}{R}\ ,\ r = R\ , \tag{2}$$

and the condition specifying zero pressure jump across the interface is

$$\frac{Q_i^2 - Q_{i\infty}^2}{Q_o^2 - 1} = M_{o\infty}^2 a_{i\infty}^2 \quad , \tag{3}$$

where Q is the magnitude of the velocity $\underset{\sim}{Q}$ and a is the sound speed normalized by the freestream flow speed.

The continuity equation governs the flow in the outer region, while the continuity equation in addition to the Euler equations governs the flow in the inner region in general. The continuity equation is

$$\nabla \cdot (\rho \underset{\sim}{Q}) = 0 \quad , \tag{4}$$

or $$\frac{\partial}{\partial z}(\rho U) + \frac{1}{r}\frac{\partial}{\partial r}(r\rho V) + \frac{1}{r}\frac{\partial}{\partial \theta}(\rho W) = 0 \ ,$$

where ρ, the density normalized by the freestream density, is given by

$$\rho(z,r,\theta) = \rho_\infty(\psi)\left\{1 + \frac{\gamma-1}{2} M_\infty^2(\psi)\left[1 - \frac{Q^2(z,r,\theta)}{Q_\infty^2(\psi)}\right]\right\}^{\frac{1}{\gamma-1}} , \tag{5}$$

where

$$M_\infty(\psi) = \begin{cases} Q_{i\infty}(\psi)/a_{i\infty}(\psi) & , \psi < R_\infty \\ M_{o\infty} & , \psi > R_\infty \end{cases}$$

$$\rho_\infty(\psi) = \begin{cases} \gamma p_{i\infty}(\psi)/a_{i\infty}^2(\psi) & , \psi < R_\infty \\ 1 & , \psi > R_\infty \end{cases}$$

$$a_\infty^2(\psi) = \begin{cases} (\gamma-1)\left[h_{i\infty t}(\psi) - \frac{1}{2} Q_{i\infty}^2(\psi)\right] & , \psi < R_\infty \\ 1/M_{o\infty}^2 & , \psi > R_\infty \end{cases}$$

and the unperturbed pressure $p_{i\infty}(\psi)$ is given by the relation

$$p_{i\infty} = \frac{1}{\gamma M_{o\infty}^2} e^{\nu}$$

(which satisfies the Euler equations), where

$$\nu = \int_{R_\infty}^{\psi} \frac{\gamma W_{i\infty}^2(r)}{r a_\infty^2(r)} dr \quad .$$

Here, γ is the ratio of specific heats, $\psi(z, r, \theta)$ is the radius of the streamline passing through point (z, r, θ) in the undisturbed flow region far upstream of the wing, and the pressure has been normalized by the freestream density multiplied by the square of the freestream flow speed.

In general, the velocity perturbation inside the slipstream is rotational, and a complete solution requires solving the continuity equation (Equation 4) in addition to the Euler equation

$$(\underset{\sim}{Q} \cdot \nabla) \underset{\sim}{Q} = -\frac{1}{\rho} \nabla p \quad , \quad r < R \quad , \tag{6}$$

inside the slipstream, solving the continuity equation outside the slipstream, and determining the slipstream boundary $R(z, \theta)$.

2.1 Small Perturbation Approximation

Two simplifying assumptions, under which the requirement for solving the Euler equation in the inner region is dropped, are introduced. The first assumption is that the undisturbed inner region flow is nearly uniform:

$$\frac{\sqrt{W_{i\infty}^2(r) + \Delta U_{i\infty}^2(r)}}{\overline{U}_{i\infty}} << 1 \quad ,$$

where

$$U_{i\infty}(r) = \overline{U}_{i\infty} + \Delta U_{i\infty}(r)$$

and $\bar{U}_{i\infty}$ is the average value of $U_{i\infty}(r)$. The second assumption is the small disturbance assumption which limits the wings considered here to wings with small surface slopes. To see the simplifying effects of these assumptions, take the curl of Equation (6). This gives

$$(\underset{\sim}{Q} \cdot \nabla)\underset{\sim}{\zeta} = \frac{\zeta}{\rho}(\underset{\sim}{Q} \cdot \nabla)\rho + (\underset{\sim}{\zeta} \cdot \nabla)\underset{\sim}{Q} + \frac{1}{\rho^2}(\nabla\rho \times \nabla\rho) \quad , \tag{7}$$

for $r < R$, where $\underset{\sim}{\zeta}$ is the vorticity and

$$\underset{\sim}{\zeta} = \nabla \times \underset{\sim}{Q} .$$

Under the two assumptions made above, Equation (7) to the lowest order becomes

$$\frac{\partial \underset{\sim}{\zeta}}{\partial z} = 0 .$$

This allows the velocity perturbation in the inner region to be expressed in terms of a velocity potential, and the governing equations simplify to

$$\frac{\partial}{\partial z}\left[\rho(U_\infty + \phi_z)\right] + \frac{1}{r}\frac{\partial}{\partial r}(r\rho\phi_r)$$
$$+ \frac{1}{r}\frac{\partial}{\partial \theta}\left[\rho(W_\infty + \frac{1}{r}\phi_\theta)\right] = 0 ,$$

where

$$U_\infty = \begin{cases} U_{i\infty}(r) & , r < R_\infty \\ 1 & , r > R_\infty \end{cases}$$

$$W_\infty = \begin{cases} W_{i_\infty}(r) & , r < R_\infty \\ 0 & , r > R_\infty \end{cases}$$

and ρ is given by Equation (5) with ψ replaced by r . The governing equation is further simplified by replacing the full potential equation with the transonic small disturbance equation

$$\frac{\partial}{\partial z}\left[\rho(U_\infty + \phi_z)\right] + \frac{1}{r}\frac{\partial}{\partial r}(r\rho\phi_r) + \frac{1}{r}\frac{\partial}{\partial \theta}\left(\frac{1}{r}\rho_\infty\phi_\theta\right) = 0 , \tag{8}$$

where ρ is to be approximated by the first four terms of the binomial expansion for Equation (5). The conditions at the slipstream boundary reduce to

$$\frac{\phi_r(z, R_\infty - \varepsilon, \theta)}{\phi_r(z, R_\infty + \varepsilon, \theta)} = U_{i\infty}(R_\infty) \ , \ \varepsilon \to 0 \ , \tag{9}$$

and

$$\frac{\phi_z(z, R_\infty - \varepsilon, \theta)}{\phi_z(z, R_\infty + \varepsilon, \theta)} = \frac{M_{o\infty}^2 a_{i\infty}^2(R_\infty)}{U_{i\infty}(R_\infty)} \ , \ \varepsilon \to 0 \ . \tag{10}$$

3. Numerical Approach

The solution to the governing equations is found numerically. Therefore, define a net of discrete points (z^i, r^j, θ^k) in the computational domain (see Figure 1) with

$$0 \leq i \leq I + 1 \ ,$$

$$1 \leq j \leq J + 1 \ ,$$

$$1 \leq k \leq K \ .$$

The computational domain is bounded by an outer cylindrical boundary $(r = r^{J+1})$, an upstream vertical plane $(z = z^0)$, and a downstream vertical plane $(z = z^{I+1})$. The undisturbed cylindrical slipstream boundary $(r = R_\infty)$ lies between the two cylindrical mesh surfaces $r = r^{j-1}$ and $r = r^j$, $j = j_s$, such that

$$R_\infty = \frac{r^{j_s-1} + r^{j_s}}{2} \ .$$

The wing extends in both the $\theta = \frac{\pi}{2}$ plane (which bisects the angle between the two mesh planes $\theta = \theta^k$ and $\theta = \theta^{k+1}$, $k = k_w$) and the $\theta = \frac{3\pi}{2}$ plane (which bisects the angle between the two mesh planes $\theta = \theta^k$ and $\theta = \theta^{k+1}$, $k = k_w$,).

3.1 Finite Difference Formulas

The finite difference approximation to the governing equation (Equation 8) at the point (z^i, r^j, θ^k), $1 \leq i \leq I$, $2 \leq j \leq J$, $1 \leq k \leq K$, is

$$\frac{(\tilde{\rho}^{i+\frac{1}{2},j,k}\, U^{i+\frac{1}{2},j,k}) - (\tilde{\rho}^{i-\frac{1}{2},j,k}\, U^{i-\frac{1}{2},j,k})}{z^{i+\frac{1}{2}} - z^{i-\frac{1}{2}}}$$

$$+ \frac{1}{r^j} \frac{(\rho^{i,j+\frac{1}{2},k}\, r^{j+\frac{1}{2}}\, V^{i,j+\frac{1}{2},k}) - (\rho^{i,j-\frac{1}{2},k}\, r^{j-\frac{1}{2}}\, V^{i,j-\frac{1}{2},k})}{r^{j+\frac{1}{2}} - r^{j-\frac{1}{2}}}$$

$$+ \frac{1}{r^j} \frac{(\rho_\infty{}^{i,j,k+\frac{1}{2}}\, W^{i,j,k+\frac{1}{2}}) - (\rho_\infty{}^{i,j,k-\frac{1}{2}}\, W^{i,j,k-\frac{1}{2}})}{\theta^{k+\frac{1}{2}} - \theta^{k-\frac{1}{2}}} = 0 \ , \qquad (11)$$

where

$$U^{i,j,k} = U_\infty(r^j) + u^{i,j,k} \quad ,$$

$$V^{i,j,k} = v^{i,j,k} \quad ,$$

$$W^{i,j,k} = W_\infty(r^j) + w^{i,j,k} \quad ,$$

and $f^{i,j,k}$ denotes an approximation to the function $f(z^i, r^j, \theta^k)$. The discretized density is first evaluated at points $(x^{i\pm\frac{1}{2}}, r^j, \theta^k)$. The value of $\rho^{i,j\pm\frac{1}{2},k}$ is then calculated using the relation

$$\rho^{i,j\pm\frac{1}{2},k} = \tfrac{1}{4}\left(\rho^{i-\frac{1}{2},j,k} + \rho^{i-\frac{1}{2},j\pm1,k} + \rho^{i+\frac{1}{2},j,k} + \rho^{i+\frac{1}{2},j\pm1,k}\right) .$$

The modified density, $\tilde{\rho}^{i+\frac{1}{2},j,k}$, is given by

$$\tilde{\rho}^{i+\frac{1}{2},j,k} = \rho^{i+\frac{1}{2},j,k} + \Delta\rho^{i+\frac{1}{2},j,k}$$

with
$$\Delta\rho^{i+\frac{1}{2},j,k} = -\mu^{\hat{i},j,k}(\rho^{i+\frac{1}{2},j,k} - \rho^{i-\frac{1}{2},j,k}) \quad , \tag{12}$$

where
$$\hat{i} = \begin{cases} i & , \mu^{i+2} = 0 \\ i+\frac{1}{2} & , \mu^{i+2} \neq 0 \end{cases} ,$$

and the switching function μ is given by

$$\mu = \max\left[0, \left(1 - \frac{a^2}{Q^2}\right)\right] .$$

The evaluation of the modified density $\tilde{\rho}$ at points in the constant $z^{i+\frac{1}{2}}$ plane, as done here and by Jameson (1976), produces sharper shocks than those produced by the evaluation of $\tilde{\rho}$ at constant z^i planes, as suggested by Hafez, et al., (1978). The switching function μ in Equation (12) is evaluated at the point $z^{\hat{i},j,k}$. The evaluation of the

switching function at the point $z^{i,j,k}$, as done by Jameson (1976), produces here a nonsmooth solution at the sonic line.

The artificial viscosity

$$T^{i,j,k} = \frac{(\Delta\rho^{i+\frac{1}{2},j,k}\, U^{i+\frac{1}{2},j,k}) - (\Delta\rho^{i-\frac{1}{2},j,k}\, U^{i-\frac{1}{2},j,k})}{z^{i+\frac{1}{2}} - z^{i-\frac{1}{2}}} ,$$

which is an approximation to

$$- \frac{\partial}{\partial z} (U\mu\rho_z \Delta z)$$

(where Δz is the mesh spacing in the z direction), has been added to the central difference approximation to Equation (4) in order to produce a stable difference scheme in the supersonic zone. This form for the viscosity was introduced by Jameson (1976) to solve the full potential equation in conservative form. Since the flow is nearly aligned with the z coordinate, it is sufficient to add the viscosity to the z derivative only.

The perturbation velocity components $u^{i+\frac{1}{2},j,k}$ and $u^{i-\frac{1}{2},j,k}$ are defined by the formulas

$$u^{i+\frac{1}{2},j,k} = \frac{\phi^{i+1,j,k} - \phi^{i,j,k}}{z^{i+1} - z^{i}}$$

and

$$u^{i-\frac{1}{2},j,k} = \frac{\phi^{i,j,k} - \phi^{i-1,j,k}}{z^{i} - z^{i-1}} .$$

Similar formulas for $v^{i,j+\frac{1}{2},k}$ and $v^{i,j-\frac{1}{2},k}$ are used at all mesh points except those where $j = j_s - 1$ and $j = j_s$, respectively. The appropriate formulas at these points are derived in Appendix A and are given by

$$v^{i,(j-1)+\frac{1}{2},k} = \frac{2\,(B\phi^{i,j,k} - \phi^{i,j-1,k})}{(r^{j} - r^{j-1})\,(1 + AB)} , \quad j = j_s , \qquad (13)$$

for points in the inner region at the slipstream boundary, and

$$v^{i,j-\frac{1}{2},k} = \frac{2A(B\phi^{i,j,k} - \phi^{i,j-1,k})}{(r^j - r^{j-1})\ (1 + AB)}\ , \quad j = j_s\ , \tag{14}$$

for points in the outer region at the slipstream boundary, where

$$A = \frac{1}{U_{i\infty}(R_\infty)}$$

and

$$B = M^2_{o\infty} a^2_{i\infty}(R_\infty)\ .$$

The perturbation velocity components $w^{i,j,k+\frac{1}{2}}$ and $w^{i,j,k-\frac{1}{2}}$ are defined by the formulas

$$w^{i,j,k+\frac{1}{2}} = \frac{1}{r^j}\ \frac{\phi^{i,j,k+1} - \phi^{i,j,k}}{\theta^{k+1} - \theta^k}$$

and

$$w^{i,j,k-\frac{1}{2}} = \frac{1}{r^j}\ \frac{\phi^{i,j,k} - \phi^{i,j,k-1}}{\theta^k - \theta^{k-1}}$$

at all points except those on the wing surface and those in the wing wake. On the wing surface the small disturbance boundary condition

$$w = U_\infty\left(\frac{\partial s}{\partial x} - \frac{W_\infty(r)}{U_\infty(r)}\right) \tag{15}$$

is used, where s is the deviation of the wing surface from a horizontal plane and is defined to be positive in the direction of increasing θ. The potential function ϕ is discontinuous at the wing wake. There, the following formulas are used:

$$w^{i,j,k+\frac{1}{2}} = \frac{1}{r^j}\ \frac{\phi^{i,j,k+1} + c^j - \phi^{i,j,k}}{\theta^{k+1} - \theta^k}\ , \quad k = k_w$$

$$w^{i,j,k-\frac{1}{2}} = \frac{1}{r^j}\ \frac{\phi^{i,j,k} - (\phi^{i,j,k-1} - c^j)}{\theta^k - \theta^{k-1}}\ , \quad k = k_w + 1$$

$$w^{i,j,k+\frac{1}{2}} = \frac{1}{r^j}\ \frac{\phi^{i,j,k+1} - c^j - \phi^{i,j,k}}{\theta^{k+1} - \theta^k}\ , \quad k = k_w,$$

$$w^{i,j,k-\frac{1}{2}} = \frac{1}{r^j} \frac{\phi^{i,j,k} - (\varphi^{i,j,k-1} + C'^j)}{\theta^k - \theta^{k-1}} \quad , \quad k = k_w, +1$$

where

$$C^j = \phi^j_{u,\frac{\pi}{2}} - \phi^j_{\ell,\frac{\pi}{2}} \quad ,$$

$$C'^j = \phi^j_{u,\frac{3\pi}{2}} - \phi^j_{\ell,\frac{3\pi}{2}} \quad ,$$

and $\phi^j_{u,\frac{\pi}{2}}$, $\phi^j_{\ell,\frac{\pi}{2}}$ are, respectively, the values of the potential ϕ at the upper and lower surfaces of the wing trailing edge located at $\theta = \frac{\pi}{2}$, $r = r^j$, and $\phi^j_{u,\frac{3\pi}{2}}$, $\phi^j_{\ell,\frac{\pi}{2}}$ are respectively the values of the potential ϕ at the upper and lower surfaces of the wing trailing edge located at $\phi = \frac{3\pi}{2}$, $r = r^j$.

The far field boundary conditions are given by

$$u^{0,j,k} = 0$$

and

$$\phi^{i,J+1,k} = 0 \quad ,$$

and on the downstream plane $(z = z^{I+1})$, Equation (11) is solved with the z derivative in that equation set equal to zero.

3.2 Finite Difference Formulas at the Axis

Define a Cartesian coordinate system (x, y, z) with a horizontal x-axis $(\theta = \frac{\pi}{2})$ and a vertical y-axis $(\theta = 0)$. The continuity equation in Cartesian coordinates is

$$\frac{\partial}{\partial z}\left[\rho(U_\infty + \phi_z)\right] + \frac{\partial}{\partial x}(\rho_\infty \phi_x) + \frac{\partial}{\partial y}(\rho_\infty \phi_y) = 0 \quad . \qquad (16)$$

The finite difference approximation to Equation (16) is used for points along the z-axis and is given by

$$\frac{(\tilde{\rho}U)^{i+\frac{1}{2},j,k} - (\tilde{\rho}U)^{i-\frac{1}{2},j,k}}{z^{i+\frac{1}{2}} - z^{i-\frac{1}{2}}}$$

$$+ \frac{(\rho V_c)^{i,j+\frac{1}{2},k_w+\frac{1}{2}} - (\rho V_c)^{i,j+\frac{1}{2},k_w'+\frac{1}{2}}}{\Delta x}$$

$$+ \frac{(\rho_\infty W_c)^{i,j+\frac{1}{2},T} - (\rho_\infty W_c)^{i,j+\frac{1}{2},B}}{\Delta y} = 0 , \qquad (17)$$

where

$$V_c = \phi_x ,$$

$$W_c = \phi_y ,$$

$$( )^{i,j+\frac{1}{2},T} = \frac{1}{2}\left[( )^{i,j+\frac{1}{2},k_w} + ( )^{i,j+\frac{1}{2},k_w'+1} \right],$$

$$( )^{i,j+\frac{1}{2},B} = \frac{1}{2}\left[( )^{i,j+\frac{1}{2},k_w+1} + ( )^{i,j+\frac{1}{2},k_w'} \right],$$

and Δx , Δy are the mesh spacings in the x and y directions, respectively. The potential function ϕ is double valued at the axis. As the axis is approached from above, it takes a value ϕ^+ and as it is approached from below it takes another value ϕ^- . Therefore, set

$$\phi^{i,1,k} = \begin{cases} \phi^{i+} \begin{cases} , & 0 < \theta_k < \frac{\pi}{2} \\ , & \frac{3\pi}{2} < \theta_k < 2\pi \end{cases} \\ \\ \phi^{i-} \quad , \quad \frac{\pi}{2} < \theta_k < \frac{3\pi}{2} \end{cases}$$

and express the velocity components U , V_c , and W_c in terms of the potential function ϕ by formulas similar to those used for mesh points away from the axis.

3.3 Iterative Procedure

Equation (11) written at all mesh points off the axis and Equation (17) written for all mesh points on the axis constitute a nonlinear system of algebraic equations for the potential function $\phi^{i,j,k}$ at the mesh points. Hafez, et al., (1978) and Holst (1979) have recently solved the transonic full potential equation by a simple line relaxation scheme which requires no special treatment for supersonic points. This simple scheme is used here. The finite difference equations at all mesh points may be written in the form

$$\underset{\sim}{E}^{j,k} = 0 \qquad \begin{matrix} , \ j = 1, 2, \ldots , J \\ , \ k = 1, 2, \ldots , K \end{matrix} \qquad (18)$$

where $\underset{\sim}{E}^{j,k}$ is an I-component vector whose i^{th} element is given by the left hand side of Equation (11) if $j > 1$ and is given by the left hand side of Equation (17) if $j = 1$. When the velocity components appearing explicitly in the finite difference equations are expressed in terms of the velocity potential the vector $\underset{\sim}{E}^{j,k}$ can be split in the following manner

$$\underset{\sim}{E}^{j,k} = D^{j,k} \, \underset{\sim}{\phi}_*^{j,k} - \underset{\sim}{f}^{j,k} \qquad \begin{matrix} , \ j = 1, 2, \ldots , J \\ , \ k = 1, 2, \ldots , K \end{matrix} \qquad (19)$$

where the vector $\underset{\sim}{\phi}_*^{j,k}$ is given by

$$\underset{\sim}{\phi}_*^{j,k} = \begin{bmatrix} \phi^{1,j,k} \\ \phi^{2,j,k} \\ \cdot \\ \cdot \\ \cdot \\ \phi^{I,j,k} \end{bmatrix}.$$

In order to solve Equation (18) iteratively, a sequence of vectors $\underset{\sim}{\phi}_{*n}^{j,k}$, $n = 1, 2, \ldots$ is defined. These vectors are obtained by solving the linear system of algebraic equations

$$D_{n-1}^{j,k} \ \underset{\sim}{\phi}_{*n}^{j,k} = \underset{\sim}{f}_{n,n-1}^{j,k} \qquad \begin{matrix} , \ j = 1, 2, \ldots , J \\ , \ k = 1, 2, \ldots , K \end{matrix}$$

where $D^{j,k}_{n-1}$ is the matrix $D^{j,k}$ with its elements evaluated using the $n-1^{st}$ iterative solution, and $f^{j,k}_{\sim n,n-1}$ is the vector $f^{j,k}_{\sim}$ with the $n-1^{st}$ iterative solution used for evaluating the density and the last available iterative solution used for evaluating the velocity potential. The n^{th} iterative solution is given by

$$\phi^{i,j,k}_{n} = \phi^{i,j,k}_{n-1} + \omega(\phi^{i,j,k}_{*n} - \phi^{i,j,k}_{n-1})$$

where ω is a relaxation factor. The relaxation sweep is done for lines with $k = 1$ to $k = K$ on a cylindrical surface and is then continued for cylinders with increasing radii. At the end of the relaxation sweep, the jump in potential at the wing trailing edge

$$G^{j}_{*n}$$

is found and the n^{th} iterative value is defined by the relatior

$$G^{j}_{n} = G^{j}_{n-1} + \Omega(G^{j}_{*n} - G^{j}_{n-1})$$

where Ω is a relaxation factor. Relaxation sweeps of the computational domain are repeated until convergence occurs. In order to improve stability and the rate of convergence, a ϕ_{zt} term

$$-\kappa\frac{\tilde{\rho}^{i-\frac{1}{2},j,k}_{n-1}}{2}\frac{\left(\phi^{i,j,k}_{*n} - \phi^{i,j,k}_{n-1}\right) - \left(\phi^{i-1,j,k}_{*n} - \phi^{i-1,j,k}_{n-1}\right)}{(z_i - z_{i-1})\Delta t}$$

is added in the n^{th} iterative sweep to the left-hand side of the algebraic equation solved for the mesh point (i,j,k) where κ is a constant and we set

$$\Delta t = z_i - z_{i-1} .$$

4. Results

The method presented above for solving the slipstream-wing interaction problem has been used to modify a computer code developed by M. Hafez (for solving the transonic full potential equation by the artificial compressibility method, described by Hafez, et al., 1978). Numerical examples are presented here for two geometrical configurations. The first is that of a simple rectangular wing, while the second is that of a swept wing.

A computational mesh with nonuniform spacings in the θ direction and with a stretching factor

$$\xi_\theta = \frac{\theta^k - \theta^{k-1}}{\theta^{k+1} - \theta^k} \quad , \quad 0 < \theta < \frac{\pi}{2} \ ,$$

is used. The mesh is symmetric about both the horizontal and vertical planes. Inside a cylindrical region with an axis coinciding with the z-axis and with its surface and end planes containing the outermost wing tips, the mesh spacings in both the axial and radial directions are uniform. Outside this cylinder, however, the mesh spacings are nonuniform. They are stretched with a stretching factor ξ_r in the positive radial direction. Downstream of the wing the mesh spacings are stretched by the factor ξ_z in the positive z direction while they are stretched by the same factor upstream of the wing in the negative z direction. Therefore the mesh spacings increase in size as one moves away from the wing. A value of 1.1 for each of three stretching factors is used here.

The results are calculated for a freestream Mach number $M_{o\infty} = 0.8$. The slipstream swirl angle α_s and total pressure $p_{ti\infty}$ distributions of highly loaded propellers under development (see Welge and Crowder, 1978) are shown in Figures 2 and 3. These distributions are used in the calculations presented here. It is noted that Equations (13) and (14) are valid for general A and B values. However, for the $p_{ti\infty}/p_{to\infty}$ distribution of Figure 3, both A and B are approximately unity. In this case, it is consistent with the small disturbance approximation to set $A = B = 1$, allowing the problem to be solved with no special treatment for points at the slipstream boundary. Although the application of Equations (13) and (14) is a simple matter in the present calculations

where cylindrical coordinates are used, a more complex set of equations replaces them when general coordinate systems are used. In such cases, a great simplification is caused by avoiding any special treatment for points at the slipstream boundary.

The first set of results are calculated for a rectangular wing with NACA 0012 sections, a 3° angle of attack, and a maximum swirl angle $\alpha_{s\ max} = 3^{\circ}$. The rectangular wing planform is sketched in Figure 4. The calculations for the rectangular wing are carried out on a 49x20x24 (z, r, θ) mesh, with 14 mesh points along the wing chord and 20 points along the wing span. The computational mesh extends 1.5 chord lengths upstream of the wing leading edge, 5 chord lengths downstream of the wing trailing edge, and the outer cylindrical computation mesh boundary radius is 4 chord lengths. The first iterative guess is taken to be a linearly interpolated solution obtained by solving the problem on a rough mesh 40x16x16 (z, r, θ).

Profiles of the pressure coefficient

$$C_p = 2(p - p_{o\infty})$$

at sections A and B of the wing (see Figure 4) are given in Figures 5 and 6. At Section A, the swirl angle effectively reduces the wing's angle of attack. On the upper surface, the axial velocity increment in the slipstream and the swirl angle produce opposite effects. They, however, produce similar effects on the lower surface. The swirl angle tends to produce an upstream displacement in the upper surface shock position, while the axial velocity increment tends to produce a downstream displacement. At Section B, the swirl angle effectively increases the wing's angle of attack. The axial velocity increment and the swirl angle produce similar effects on the wing's upper surface and opposite effects on its lower surface. Note in Figure 6 that the slipstream effect produces a downstream displacement in the shock position, and it produces a stronger shock. This consequently contributes to an increase in the wave drag. Figures 7 and 8 show the distribution of $C_{p\ min}$ (the minimum value of C_p along a chord) along the wing span. In these figures, we see that the slipstream effect is largest inside the slipstream but extends outside it. Figure 9 shows the distribution along

the wing span of c_ℓ, the section lift coefficient. It is concluded from this figure that the slipstream effect on lift distribution is primarily due to the swirl angle.

The effect of the slipstream on the wing's wave drag is shown in Table 1. Estimates of wave drag are found (see Murman and Cole, 1974) by integrating

$$\int_{\text{shock}} \left[\!\left[\phi_z\right]\!\right]^3 ds$$

where the integral is taken along shock waves and $\left[\!\left[\phi_z\right]\!\right]$ is the jump in ϕ_z across the shock. In the table, the drag is normalized by that due to the wing semispan in the absence of the slipstream. The table shows that the swirl effect on wave drag is that of redistribution. Its effect on the total wave drag, however, is small. This is in contrast to the slipstream axial velocity which produces a large increase in wave drag.

The effect of the slipstream on the wing's lift is shown in Table 2. Estimates of lift are found by integrating twice $\Delta\phi_{te}$ (the difference in ϕ between the upper and lower wing trailing edge surfaces) along the wing span. The lift values shown in Table 2 are normalized by that due to the wing semispan in the absence of the slipstream. The table shows that the effect of the slipstream on the wing's total lift is minor.

A second example, attempting to calculate a case which is as close as possible to the experimental configuration of Welge and Crowder, (1978), is now presented. The planform of the wing-body configuration used by Welge and Crowder (1978) is depicted in Figure 10. Due to the simplicity of the computer code in the present study, it is not possible to simulate flows about complex geometries. The calculations have therefore been done for a simple swept isolated wing configuration. The wing planform is sketched in Figure 11, and the defining supercritical airfoil section is given in Table 3. This airfoil section is the same as that of the experimental wing section at the 35 percent semispan station. The use of a Cartesian coordinate system at the slipstream

axis, in the manner discussed in Section 3.2, has been found to cause solution inaccuracies near the leading edge of a swept wing. To avoid this problem, an infinite cylinder whose axis coincides with the slipstream axis is assumed. The solid wall boundary condition is applied at the cylinder's surface. The cylinder's radius is chosen to be half a mesh spacing in the radial direction. A 4.5^{o} wing angle of attack is chosen to roughly match the sectional lift coefficient in the slipstream region to that of the experimental lift coefficient in the absence of slipstream effects (swirl and axial velocity increment). In the calculations, the total pressure distribution in the slipstream is assumed to be that depicted in Figure 3. Calculations with both positive swirl angle ($\alpha_{s\ max} = 7^{o}$) and negative swirl angle ($\alpha_{s\ max} = -7^{o}$) have been performed.

The calculation for the swept wing are carried out on a 107x20x20 (z, r, θ) mesh, with 16 mesh points along the wing chord, and 20 points along the wing span. The computational mesh extends 2.5 chord lengths upstream of the wing leading tip, and 8 chord lengths downstream of the wing trailing tip, and the outer cylindrical computational mesh boundary radius is 5 chord lengths. The first iterative guess is taken to be a linearly interpolated solution obtained by solving the problem on a rough mesh 78x14x14 (z, r, θ) .

Profiles of the pressure coefficient at sections A, B, C, A', B', and C' of the wing (see Figure 11) are given in Figures 12 through 17. A comparison of the solutions at sections A and A', which are closest to the axis, indicates a strong effect due to the cylinder co-centered with the axis. The effects of this cylinder is to compress the flow at section A, and to expand the flow at section A'. These effects may be concluded from basic flow properties along swept wings and are confirmed by comparing the solutions presented in Figures 12 and 15. At sections A, B, and C, the positive (negative) swirl effectively produces a reduction (increase) in the wing's angle of attack, while the positive (negative) swirl effectively produces an increase (reduction) in the wing's angle of attack at sections A', B', and C'. Figures 18 and 19 show the distribution of $C_{p\ min}$ along the wing span, and Figure 20 shows the distribution

of the sectional lift coefficient along the wing span. The effect of the slipstream on the wing's lift is shown in Table 4. Drag calculations have not been performed, since the solutions indicate supersonic-supersonic shocks. The simple calculations which are used to estimate wave drag due to supersonic-subsonic shocks are not applicable in the case of supersonic-supersonic shocks.

Results presented in this example show similar trends (for slipstream effects on supercritical wings) to those of the experimental results produced by Welge and Crowder (1978)(see Figures 21 and 22). A qualitative comparison between the experimental results and the numerical results is not appropriate due to differences in the geometrical configurations of the experimental and numerical test cases. The absence of a body next to the wing and the presence of a cylinder in the slipstream in the calculated example, in addition to differences in the wing planform and its cross-sectional profiles between the experimental and numerical examples, contribute to differences in the flows about the experimental and numerical configurations. In addition to the current code's geometrical limitation, it should be noted that the use of the small disturbance equations near the blunt leading edge of a supercritical airfoil causes solution inaccuracies in the leading edge region. Precise numerical calculations for complex geometrical configurations may be made by the use of computer codes capable of handling these geometries. Leading-edge inaccuracies may be avoided by using full potential codes.

The calculations were done on a CDC 7600 computer. For the rectangular wing, 1 second and 2 seconds were required per iteration, respectively, on the rough mesh and the final mesh. The number of iterations required to reduce the maximum residual to 0.001 was approximately 150 for the rough mesh and 100 for the final mesh. For the swept wing, 1.36 seconds and 4.6 seconds were required per iteration, respectively, on the rough mesh and the final mesh. The number of iterations required to reduce the maximum residual to 0.001 was approximately 7[illegible] for the rough mesh and 190 for the final mesh. The values used for the relaxation factor ω varied between 1.4 and 1.6. The relaxation factor Ω for calculating the jump in potential at the trailing edge was taken to be 1.2, and K, the ϕ_{zt} term coefficient, was set equal to 1.0.

5. Concluding Remarks

In this report, an inviscid model for the interaction between a thin wing and a nearly uniform propeller slipstream has been presented. In this model, the perturbation velocities due to the interaction are potential, even though the undisturbed slipstream velocity is rotational. This allows basic information about the interaction problem to be obtained while avoiding the need for solving the Euler equations. For typical slipstream velocity distributions, only minor modifications to the free flow potential equation and wing boundary conditions are required to produce the slipstream effect. These modifications can be easily incorporated into available transonic potential codes.

The slipstream effect on a wing in the transonic regime has been demonstrated through a simple example. Solutions obtained for a rectangular wing indicate that the slipstream has a strong effect on the aerodynamic properties of the wing portion immersed in the slipstream. The effect of the slipstream on the rest of the wing is less, but it is discernable. The results indicate that the slipstream swirl has a strong effect on the wing load distribution, however, its effect on the total wing lift and wave drag is small. The axial velocity increment inside the slipstream has little effect on the wing's lift; however, it causes a large increase in wave drag.

Although the computer code used for the present study is a simple code which does not allow calculations for complex geometrical configurations, an attempt has been made to calculate a case which is as close as possible to the experimental configuration of Welge and Crowder (1978). The calculated results indicate the general trends for slipstream effects on a supercritical swept wing. However, solutions calculated are not expected to be accurate near the blunt leading edge of the supercritical wing, since the small disturbance equation is used in the present calculations. Therefore, the change in leading edge suction associated with the slipstream swirl is not properly accounted for in the solution. The computer code used in this study is a simple code for the purpose of demonstrating the interaction effects for simple geometrical configurations. More sophisticated codes are available (see Jameson and Caughey (1977) and Caughey and

Jameson (1979)) and may be used for calculating slipstream effects on wing-body combinations, provided the assumptions of a nearly uniform slipstream and a thin wing are satisfied.

References

Boctor, M. L., Clay, C. W., and Watson, C. F. (1978) "An Analysis of Prop-Fan/Airframe Aerodynamic Integration," NASA CR-152186.

Caughey, D. A., and Jameson, A. (1979) "Recent Progress in Finite Volume Calculations for Wing-Fuselage Combinations," AIAA Paper No. 79-1513.

Chow, F., Krause, E., Liu, C. H., and Mao, J. (1970) "Numerical Investigations of an Airfoil in a Nonuniform Stream," J. Aircraft 7, No. 6, 531-537.

Hafez, M. M., Murman, E. M., and South, J. C. (1978) "Artificial Compressibility Methods for Numerical Solution of Transonic Full Potential Equation," AIAA Paper No. 78-1148.

Holst, T. L. (1979) "Implicit Algorithm for the Conservative Transonic Full-Potential Equation Using an Arbitrary Mesh," AIAA Journal 17, No. 10, 1038-1045.

Jameson, A. (1976) "Numerical Computation of Transonic Flows with Shock Waves," Symposium Transsonicum II, Springer-Verlag, 384-414.

Jameson, A., and Caughey, D. A. (1977) "A Finite Volume Method for Transonic Potential Flow Calculations," Proceedings of the AIAA Third Computational Fluid Dynamics Conference.

Kleinstein, G., and Liu, C. H. (1972) "Application of Airfoil Theory for Nonuniform Streams to Wing Propeller Interaction," J. Aircraft 9, No. 2, 137-142.

Lan, C. E. (1975) "Wing-Slipstream Interaction with Mach Number Non-uniformity," J. Aircraft 12, No. 10, 759-760.

Murman, E. M., and Cole, J. D. (1974) "Inviscid Drag at Transonic Speeds," AIAA Paper No. 74-540.

Shollenberger, C. A. (1975) "Three-Dimensional Wing/Jet Interaction Analysis Including Jet Distortion Influences," J. Aircraft 12, No. 9, 706-713.

Ting, L., Liu, C. H., and Kleinstein, G. (1972) "Interference of Wing and Multipropellers," AIAA Journal 10, No. 7, 906-914.

Welge, H. R., and Crowder, J. P. (1978) "Simulated Propeller Slipstream Effects on a Supercritical Wing," NASA CR-152138.

Tables

Table 1: Normalized Wave Drag for Rectangular Wing

	Uniform Flow	Slipstream Axial Velocity Effect	Slipstream Swirl Effect	Combined Effect
Right Wing Drag	1.00	2.83	0.68	2.04
Left Wing Drag	1.00	2.83	1.48	3.82
Total Wing Drag	2.00	5.66	2.16	5.86

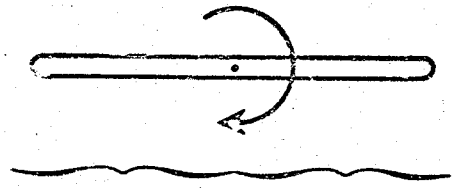

Left Wing Right Wing

Table 2: Normalized Lift for Rectangular Wing

	Uniform Flow	Slipstream Axial Velocity Effect	Slipstream Swirl Effect	Combined Effect
Right Wing Lift	1.00	1.05	0.83	0.87
Left Wing Lift	1.00	1.05	1.17	1.23
Total Wing Lift	2.00	2.10	2.00	2.10

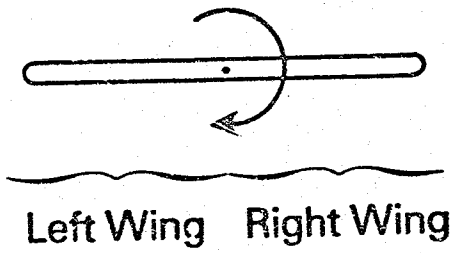

Table 3: Airfoil Section Coordinates for Swept Wing.

% Chord	Upper Surface Coordinate, y	Lower Surface Coordinate, y
0.0	−0.0568	−0.0568
0.05	−0.0540	−0.0619
0.25	−0.0491	−0.0670
0.50	−0.0455	−0.0708
1.25	−0.0393	−0.0780
2.50	−0.0327	−0.0860
5.00	−0.0245	−0.1256
7.50	−0.0189	−0.1030
10.00	−0.0144	−0.1081
15.00	−0.0079	−0.1151
20.00	−0.0033	−0.1197
25.00	0.0000	−0.1228
30.00	0.0023	−0.1250
35.00	0.0035	−0.1260
40.00	0.0041	−0.1260
45.00	0.0035	−0.1248
50.00	0.0022	−0.1223
55.00	0.0001	−0.1179
58.50	−0.0020	−0.1138
65.00	−0.0069	−0.1041
70.00	−0.0121	−0.0952
75.00	−0.0632	−0.0860
80.00	−0.0257	−0.0771
85.00	−0.0344	−0.0696
90.00	−0.0444	−0.0646
92.50	−0.0502	−0.0640
95.00	−0.0565	−0.0651
97.50	−0.0637	−0.0682
100.00	−0.0713	−0.0734

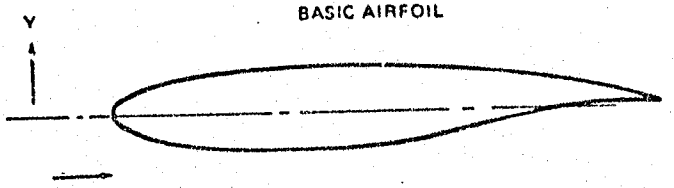

Table 4: Normalized Lift for Swept Wing

	Uniform Flow	Slipstream with Positive Swirl Angle	Slipstream with Negative Swirl Angle
Right Wing Lift	1.14	0.95	1.41
Left Wing Lift	0.86	1.13	0.63
Total Wing Lift	2.00	2.08	2.04

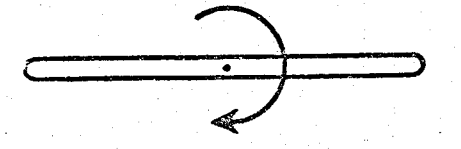

Left Wing Right Wing

Figures

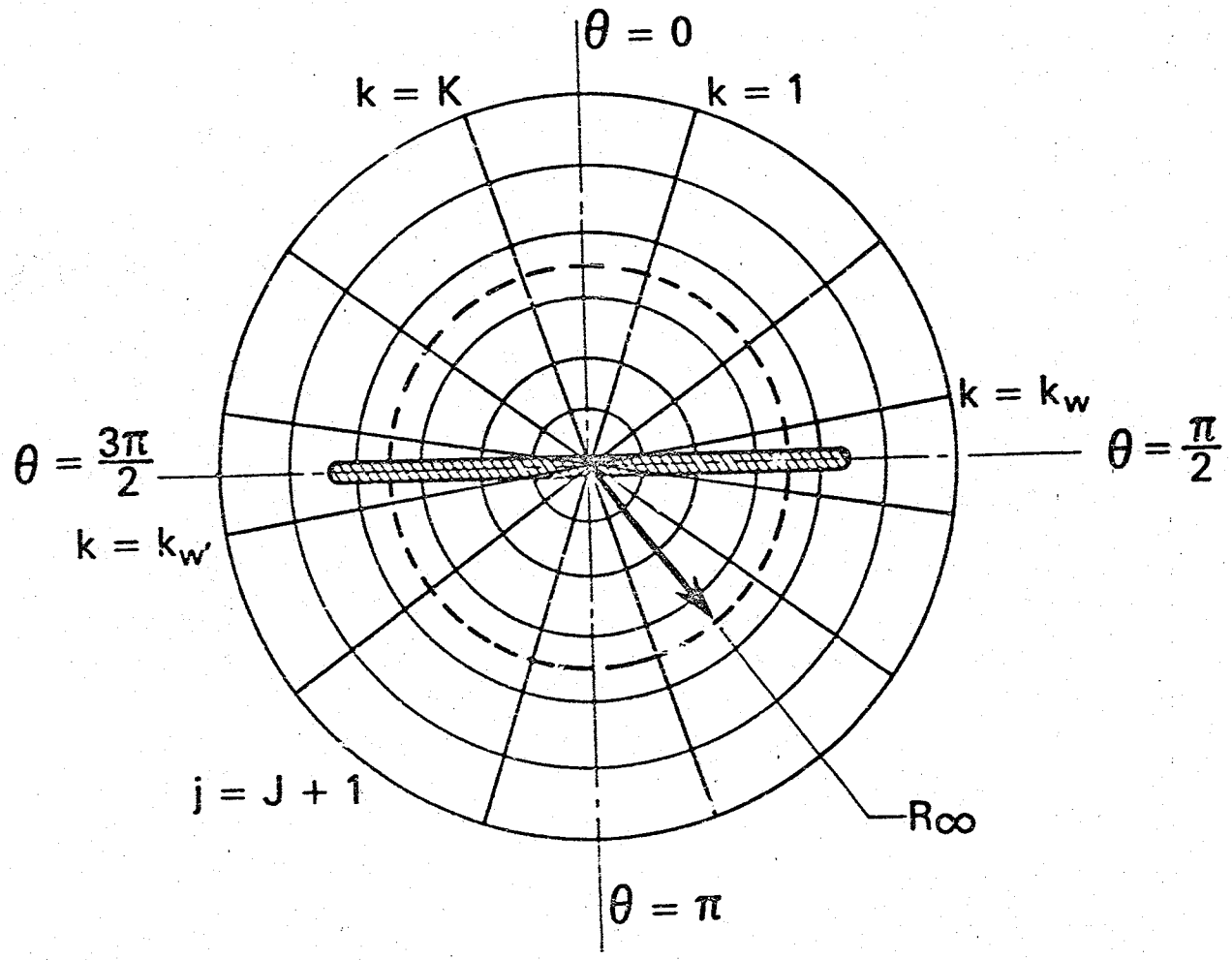

Figure 1. Cross Section Through Computational Mesh at a Constant z Plane.

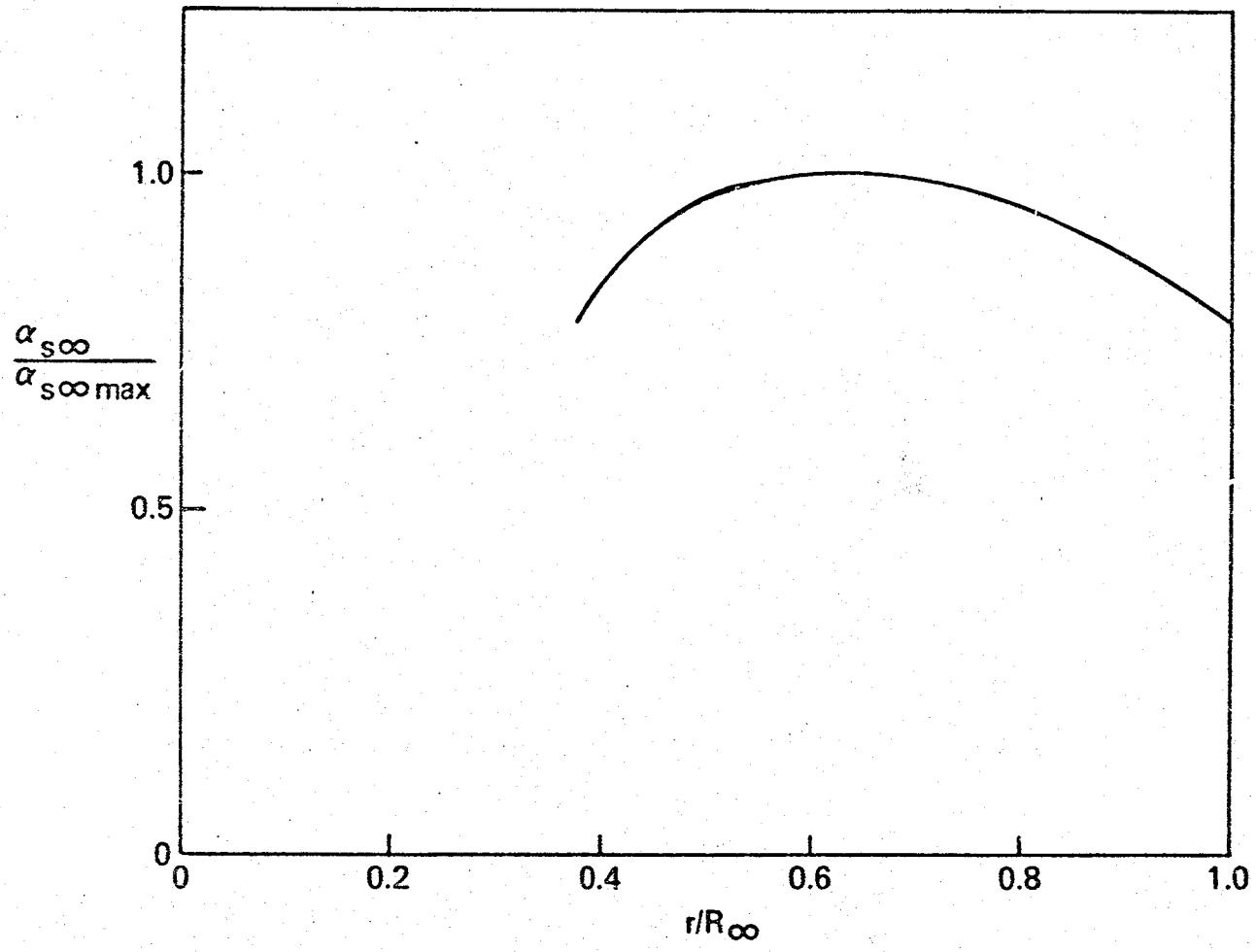

Figure 2. Swirl Angle Distribution in Undisturbed Slipstream.

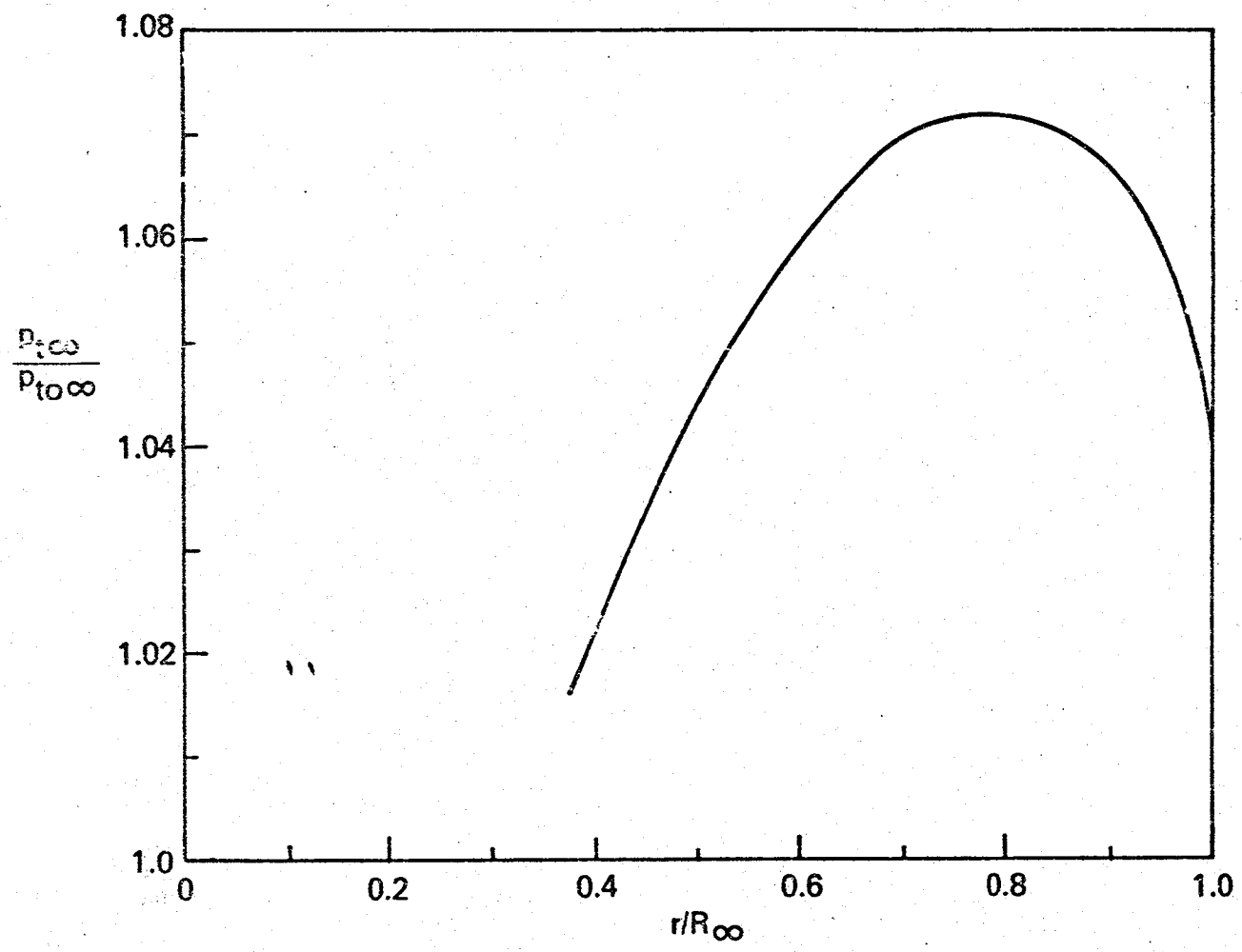

Figure 3. Total Pressure Distribution in Undisturbed Slipstream.

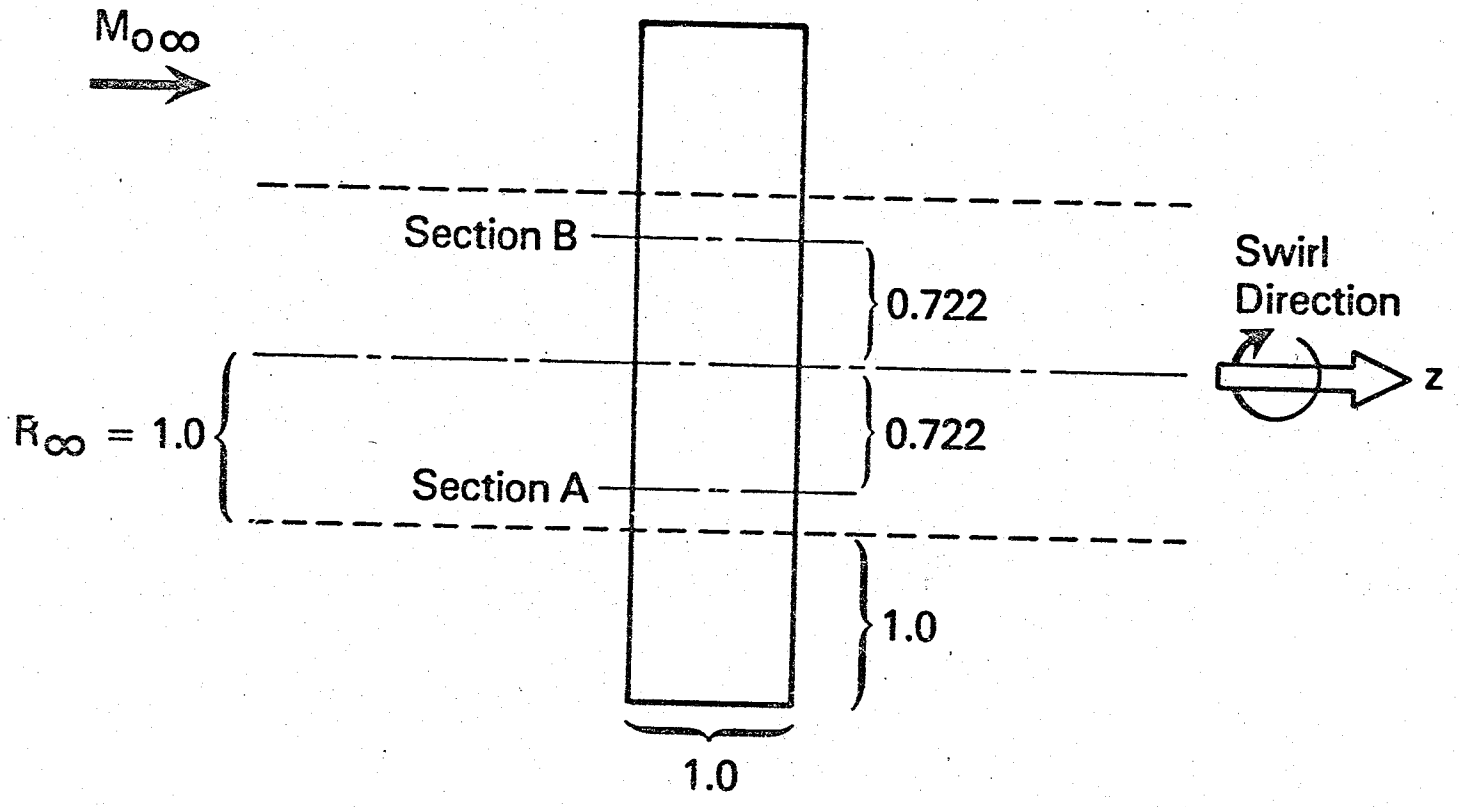

Figure 4. Rectangular Wing Planform.

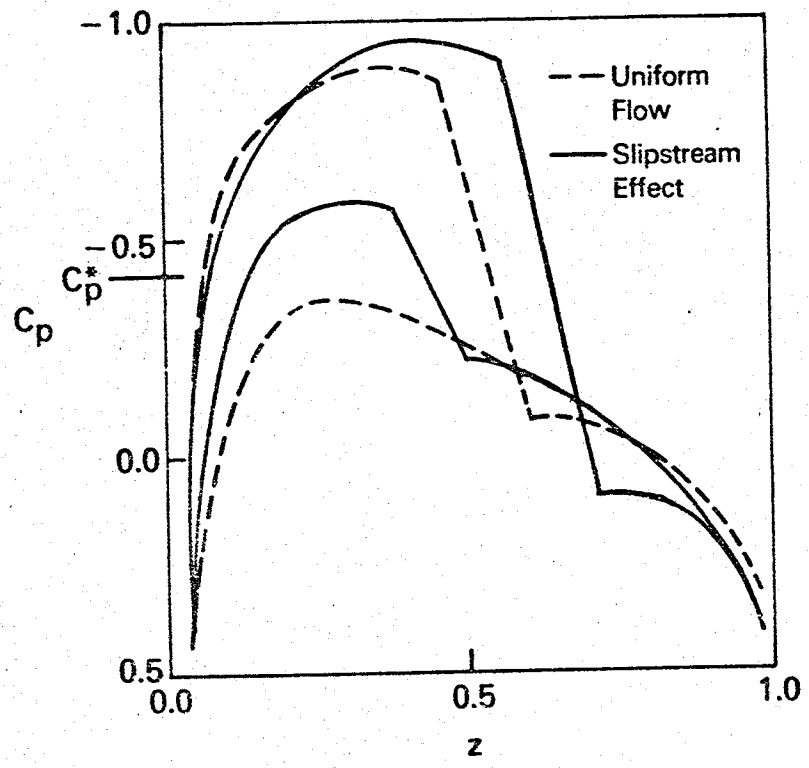

Figure 5. C_p Distribution at Section A of Rectangular Wing.

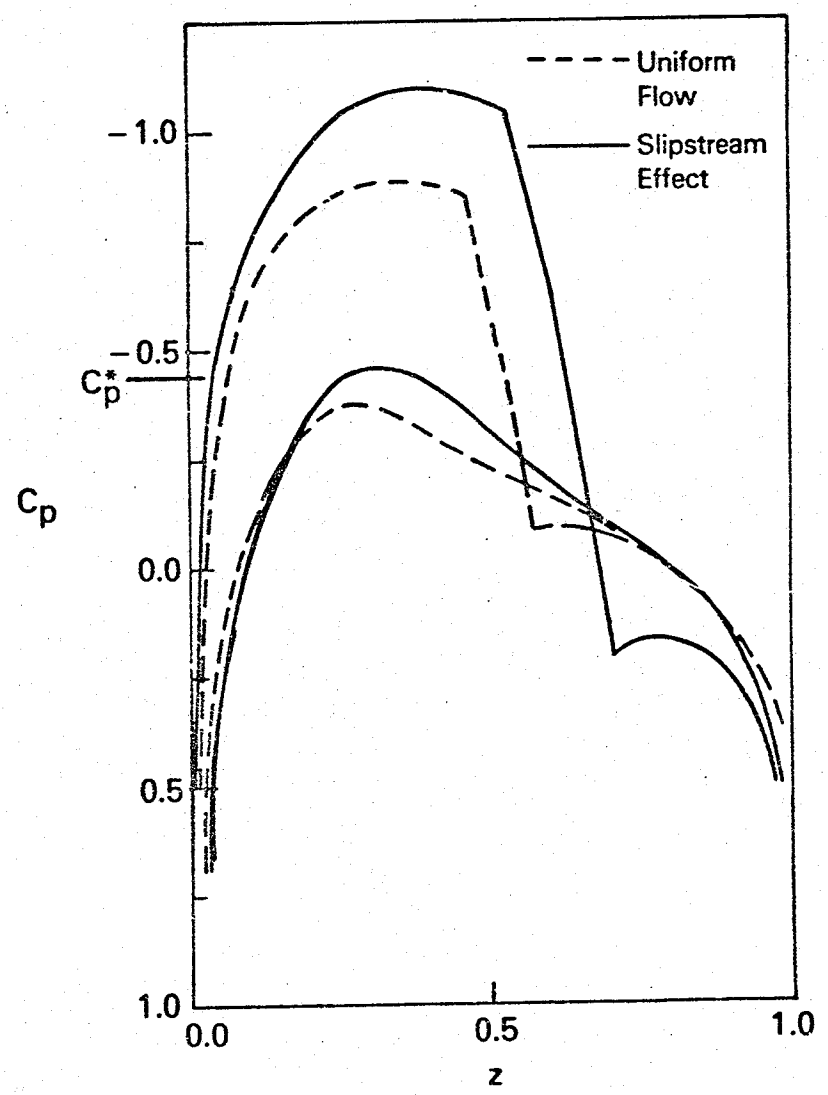

Figure 6. C_p Distribution at Section B of Rectangular Wing.

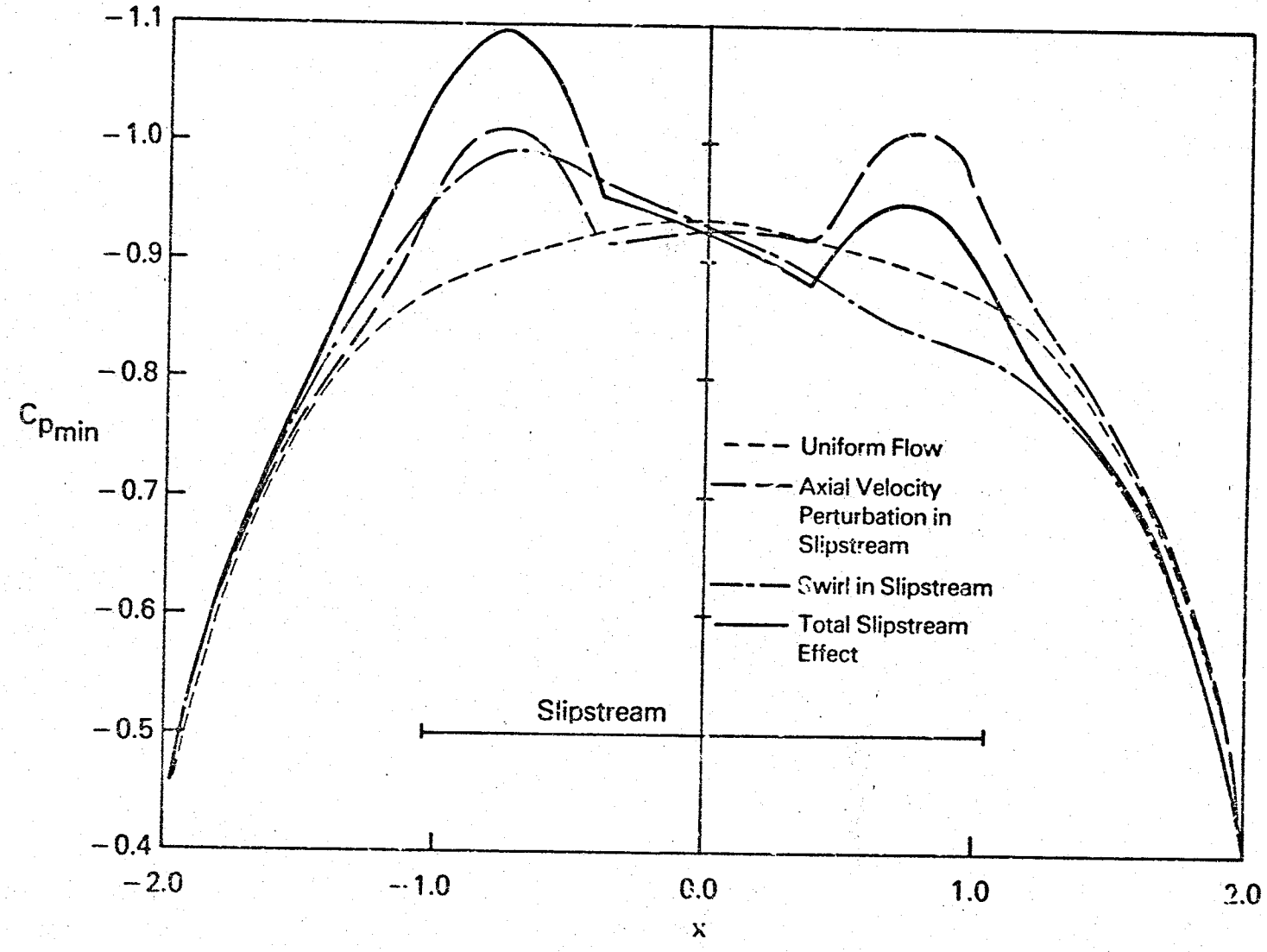

Figure 7. Minimum C_p Distribution Along Rectangular Wing Top.

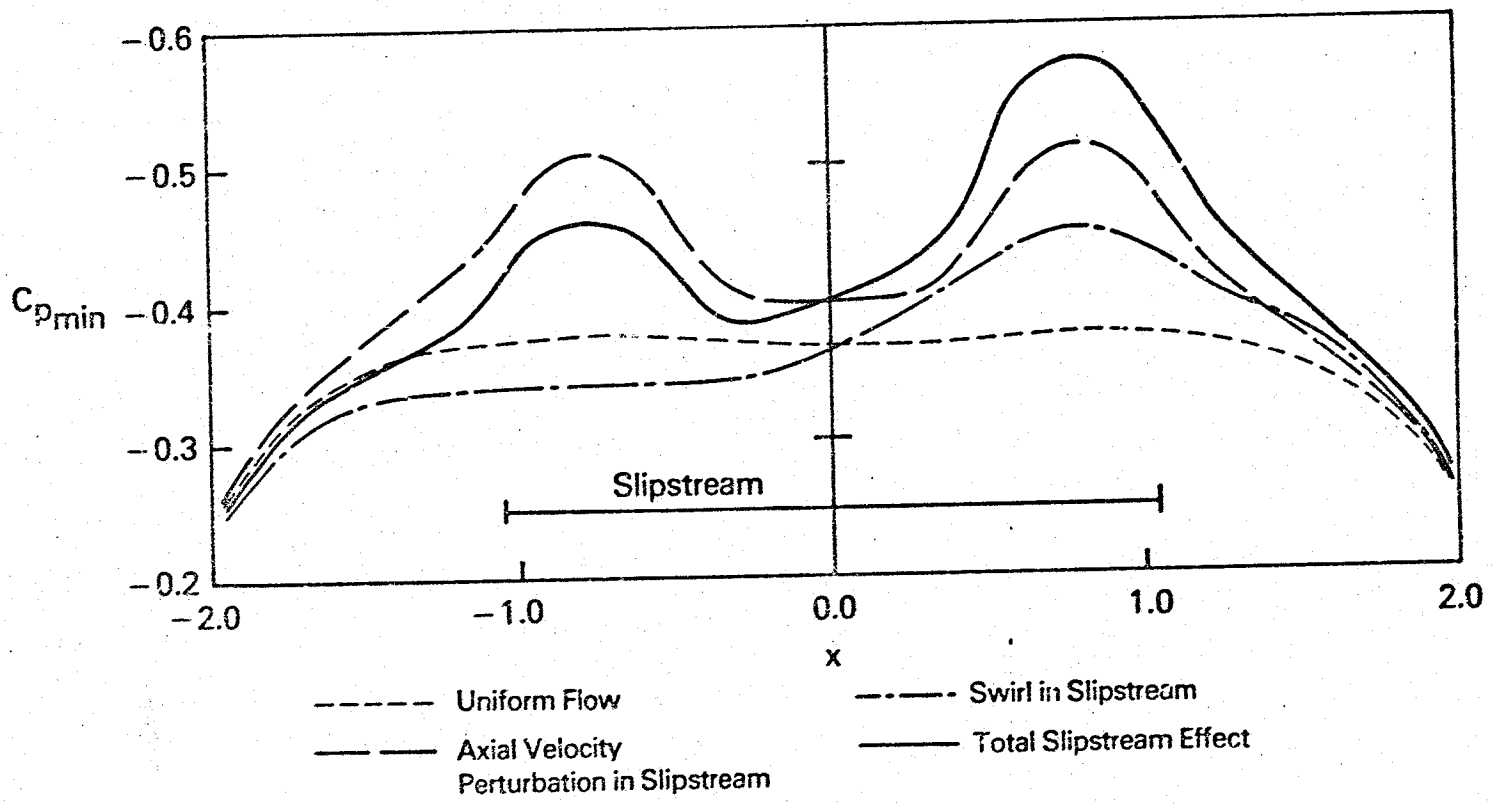

Figure 8. Minimum C_p Distribution Along Rectangular Wing Bottom.

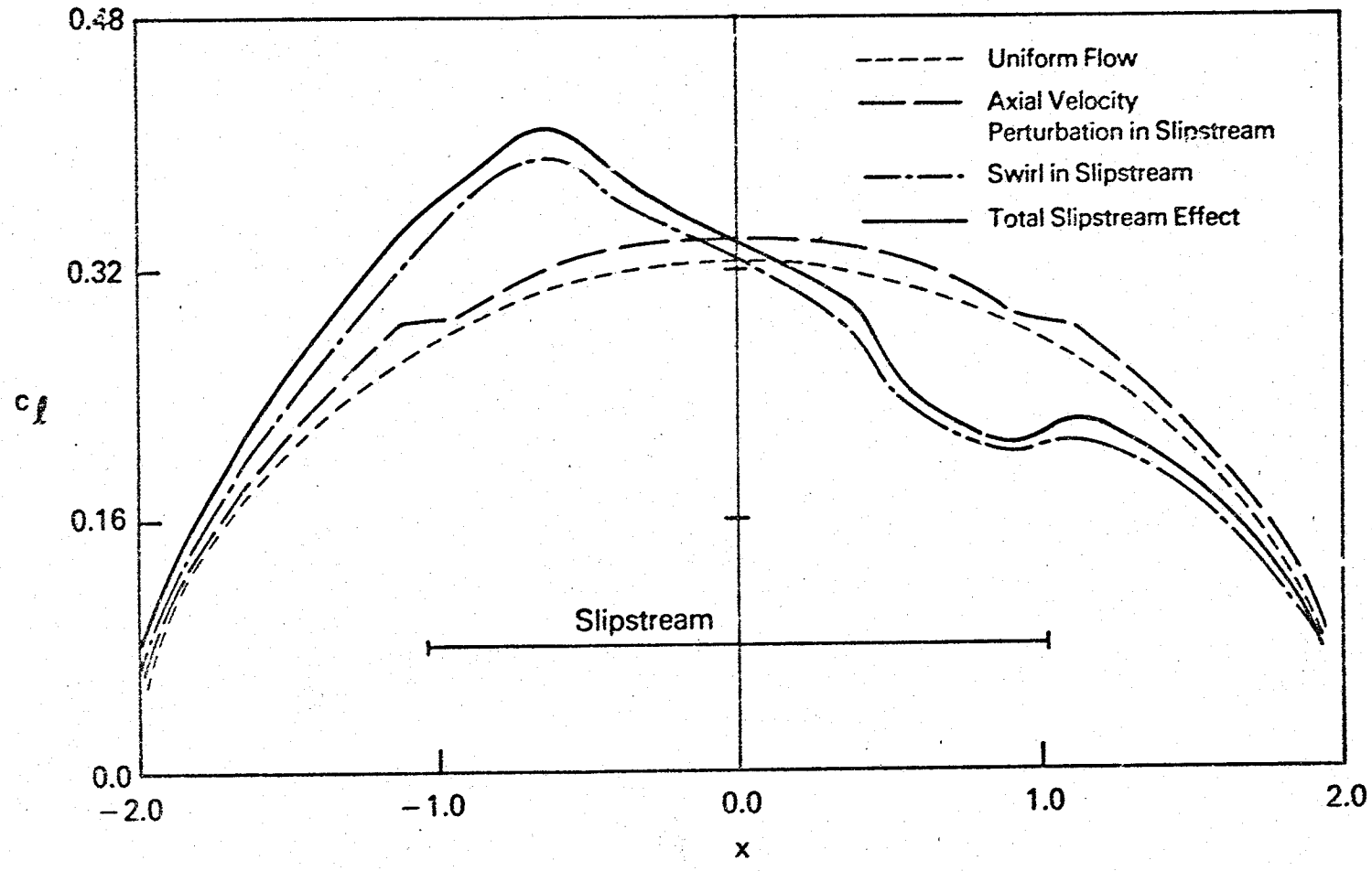

Figure 9. Lift Distribution for Rectangular Wing.

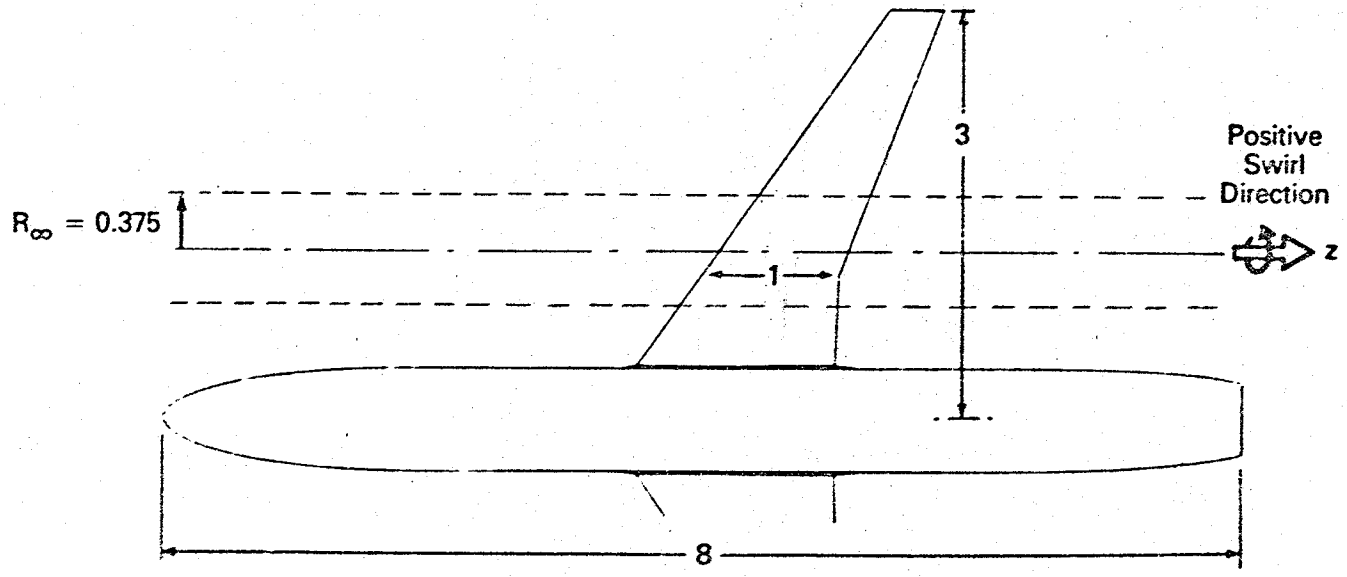

Figure 10. Illustration of Wing-Body Planform (Experimental Configuration Taken From Wedge and Crowder, 1978).

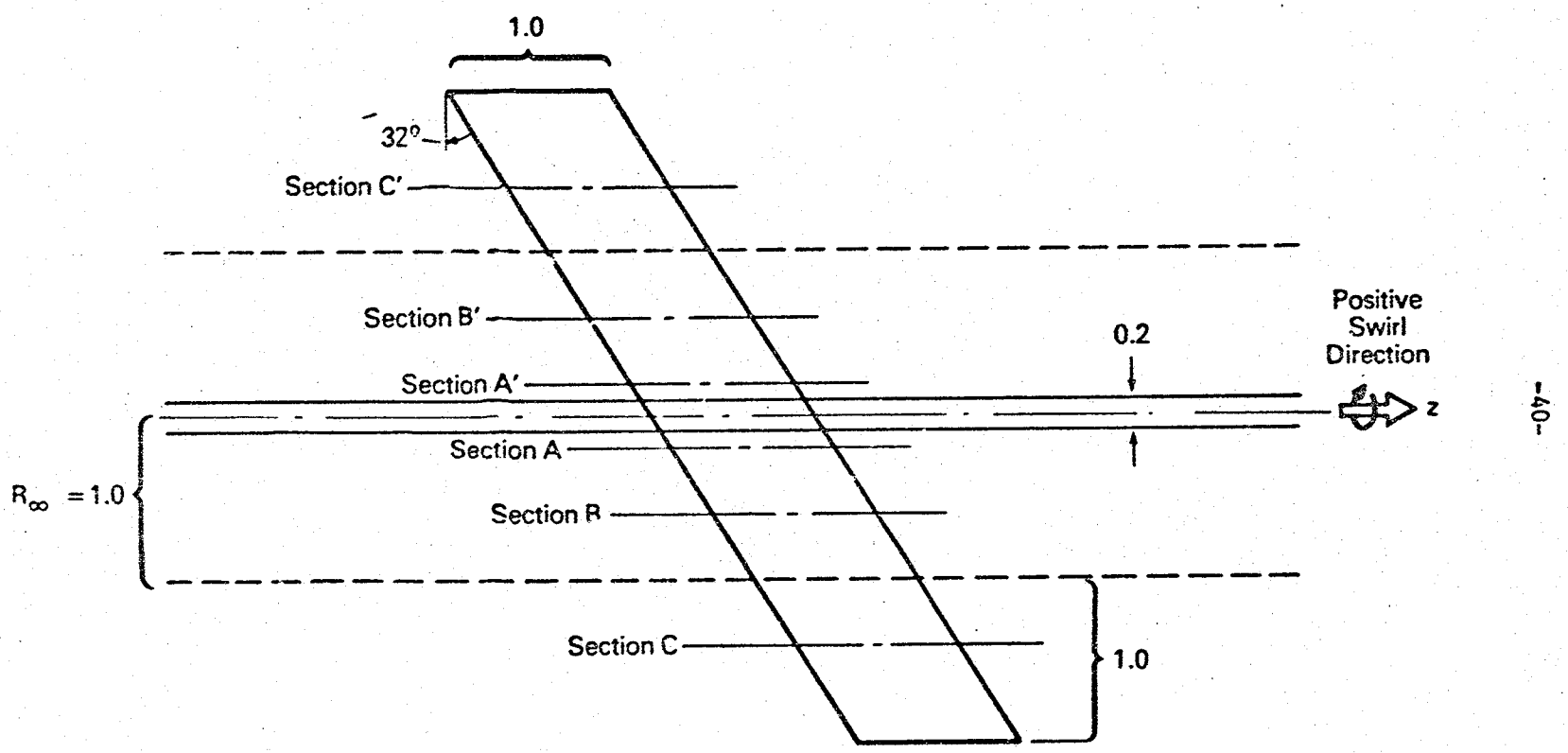

Figure 11. Swept Wing Planform.

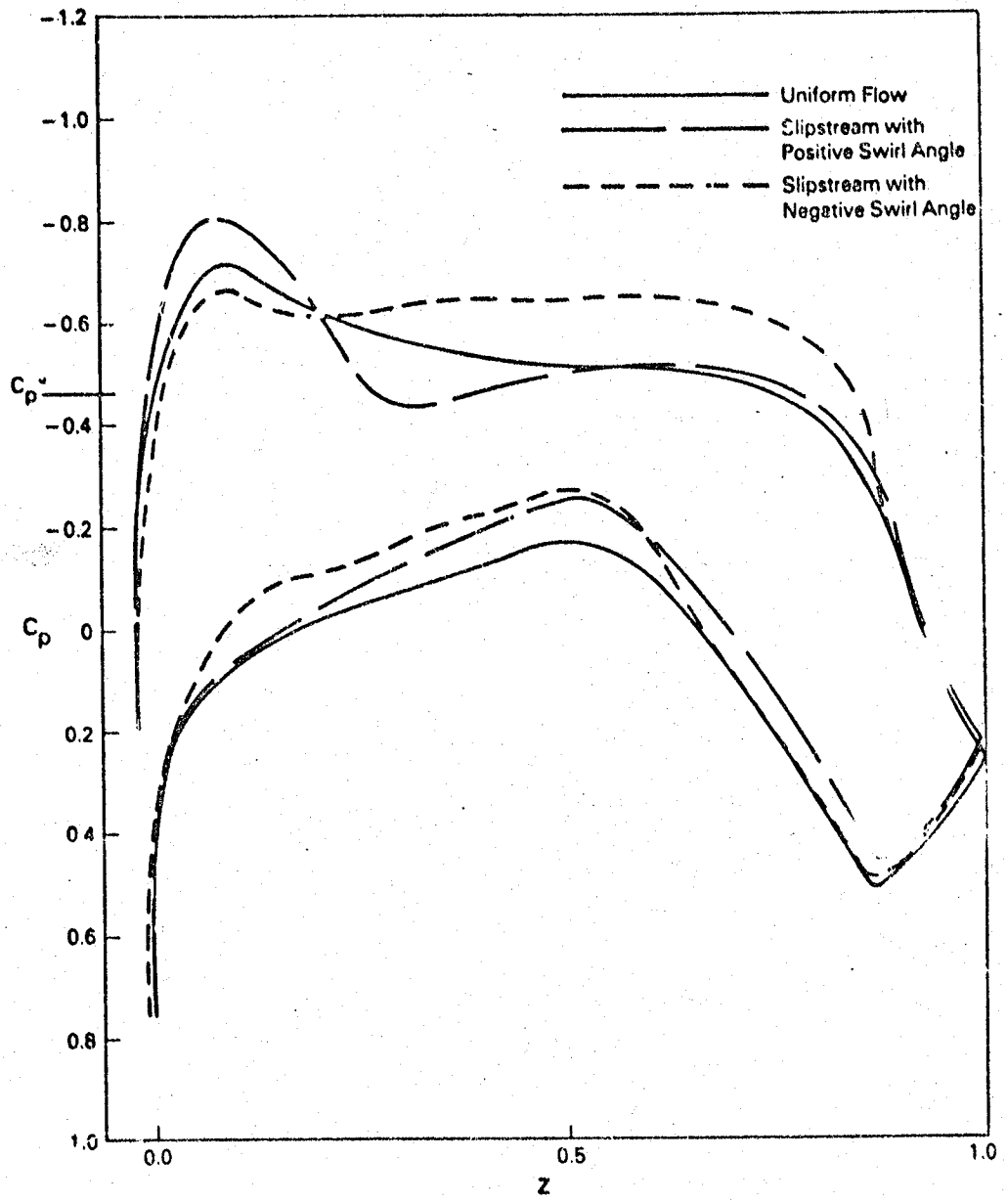

Figure 12. C_p Distribution at Section A of Swept Wing.

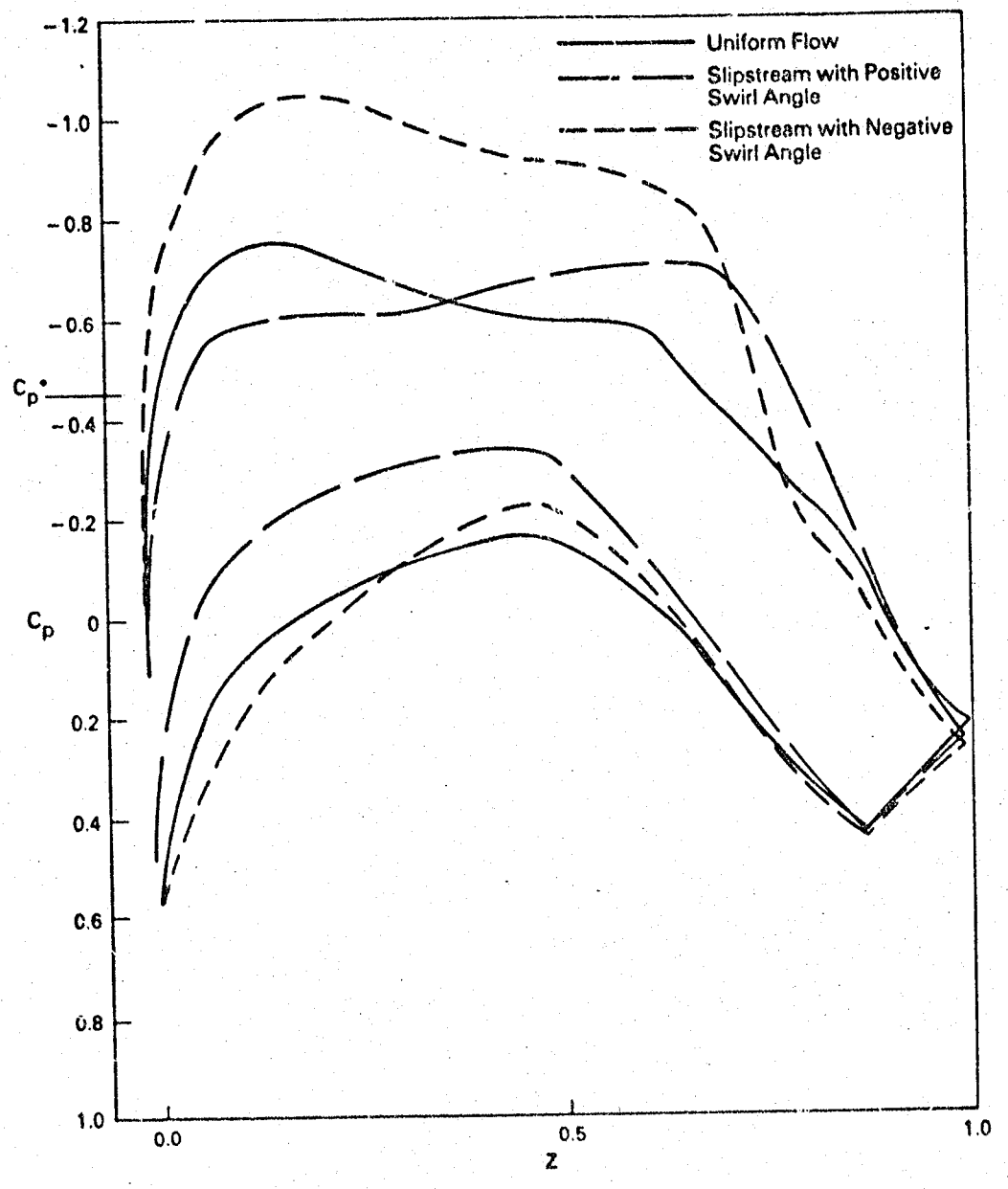

Figure 13. C_p Distribution at Section B of Swept Wing.

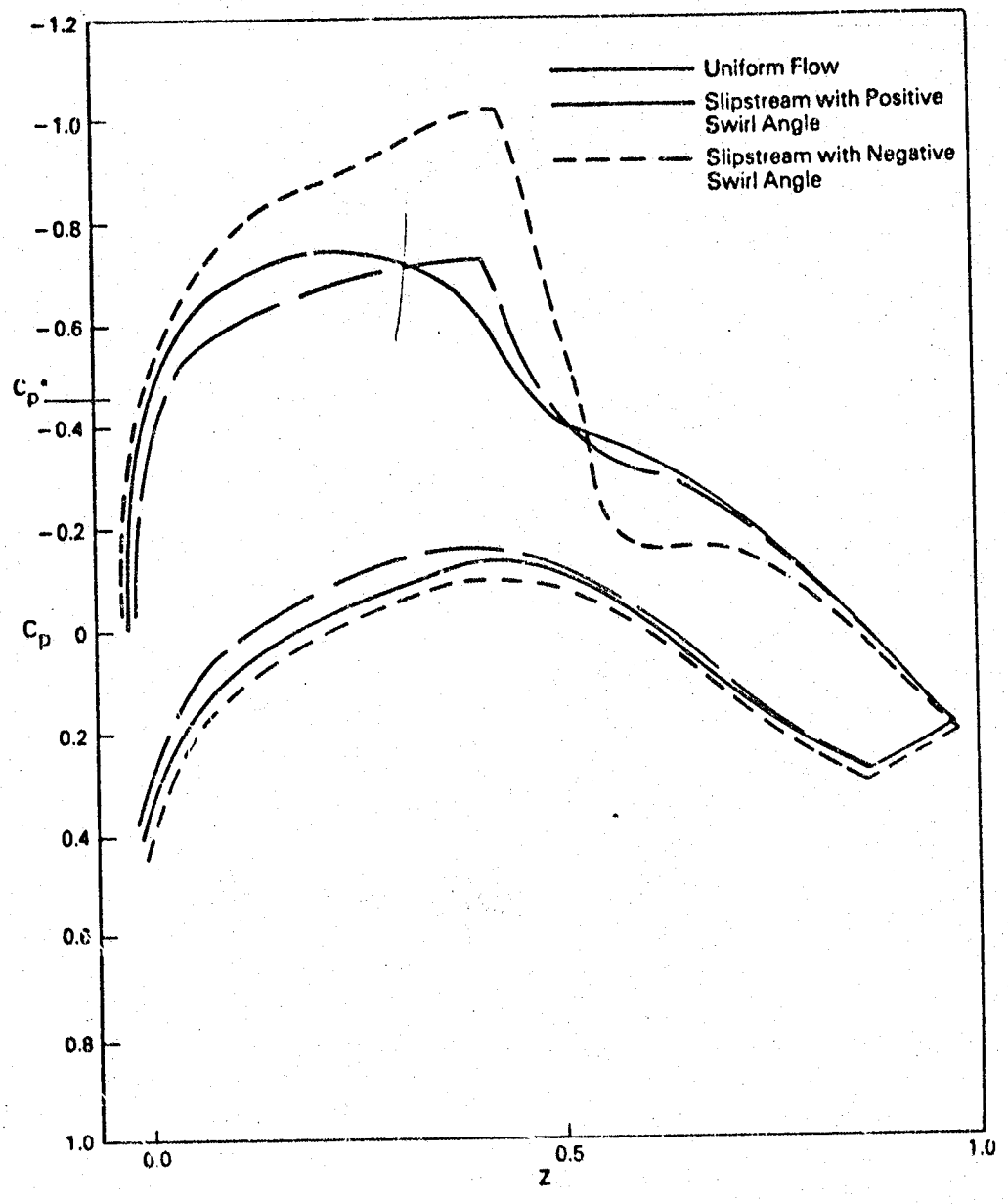

Figure 14. C_p Distribution at Section C of Swept Wing.

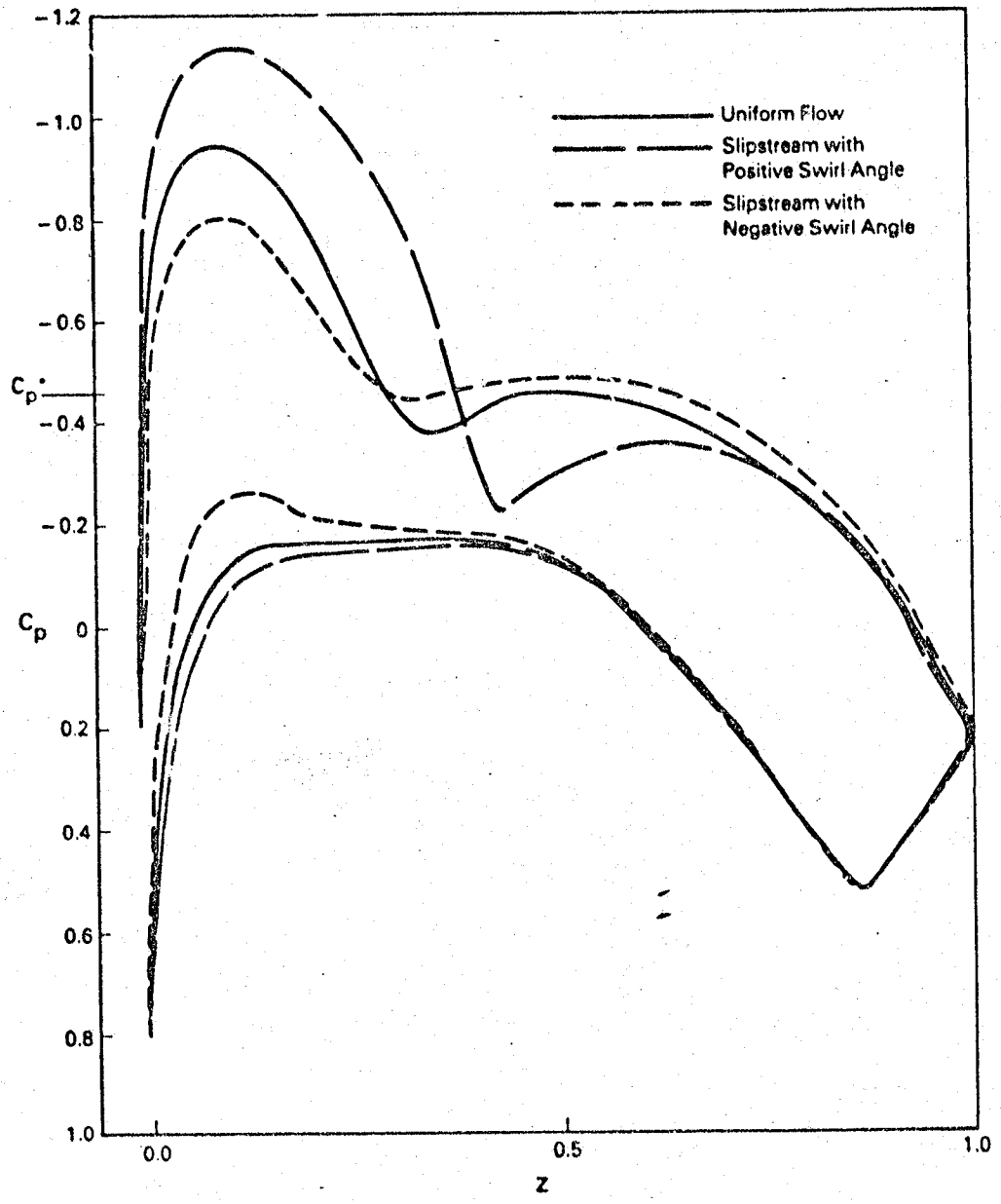

Figure 15. C_p Distribution at Section A'of Swept Wing.

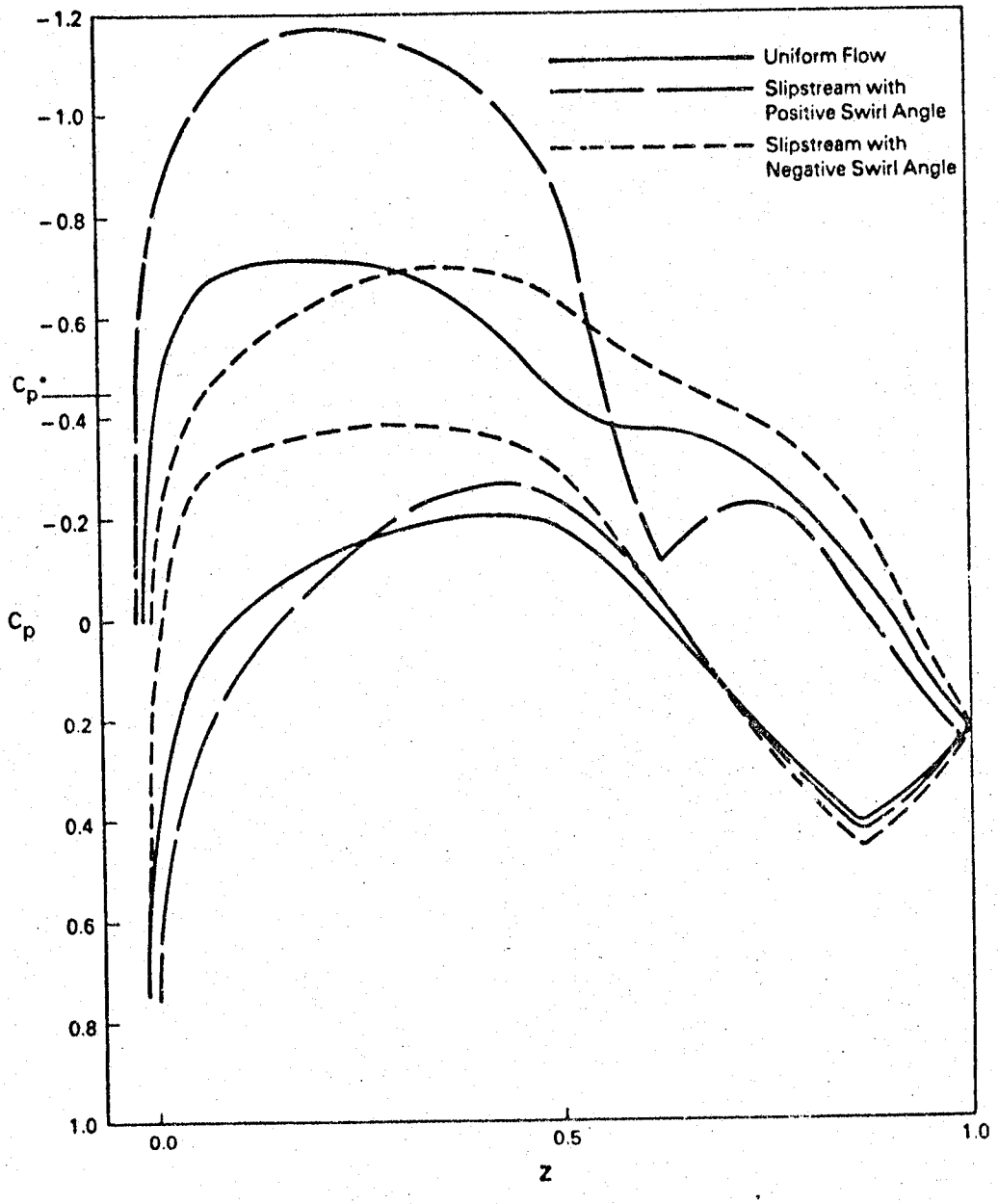

Figure 16. C_p Distribution at Section B' of Swept Wing.

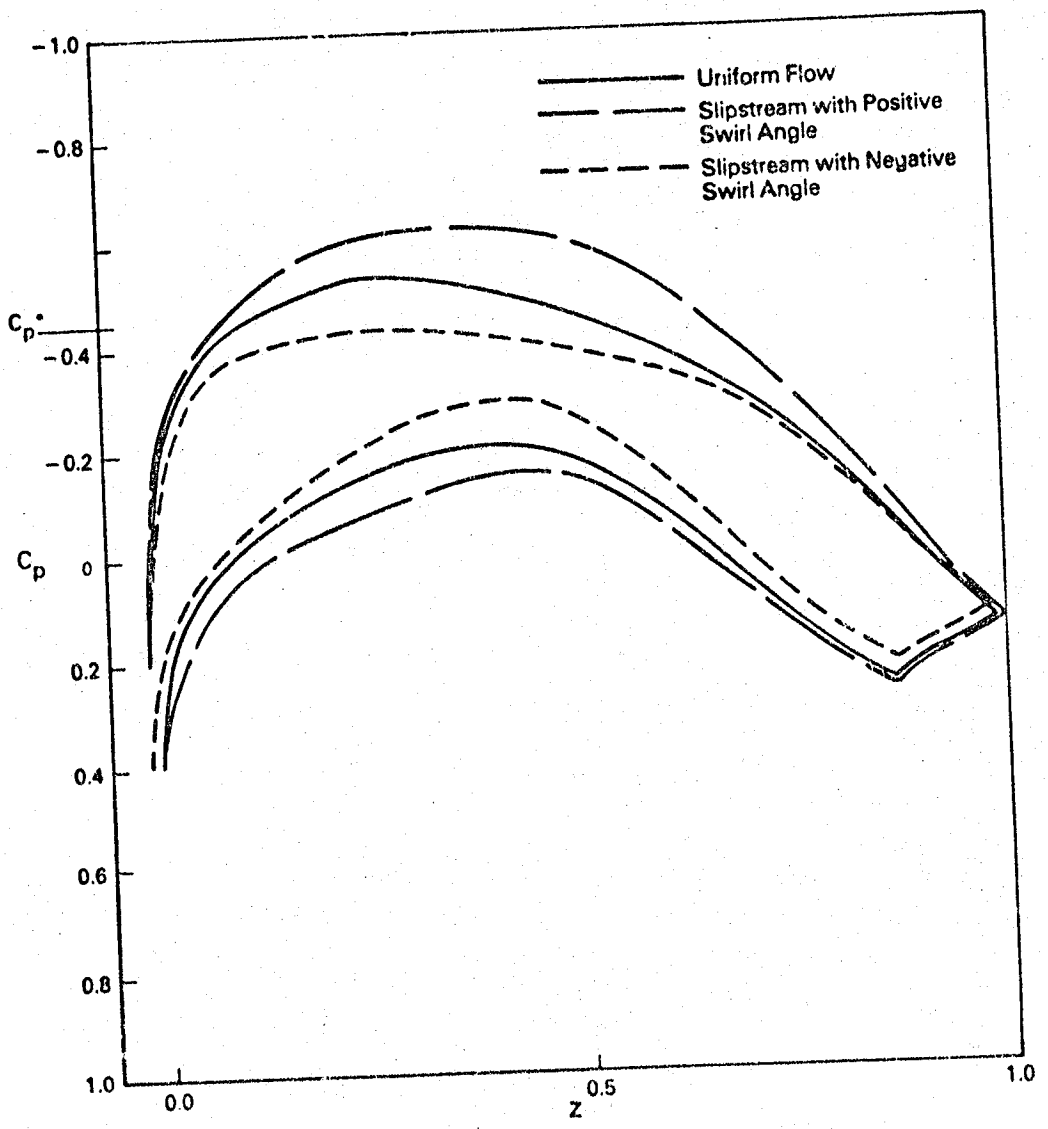

Figure 17. C_p Distribution at Section C' of Swept Wing.

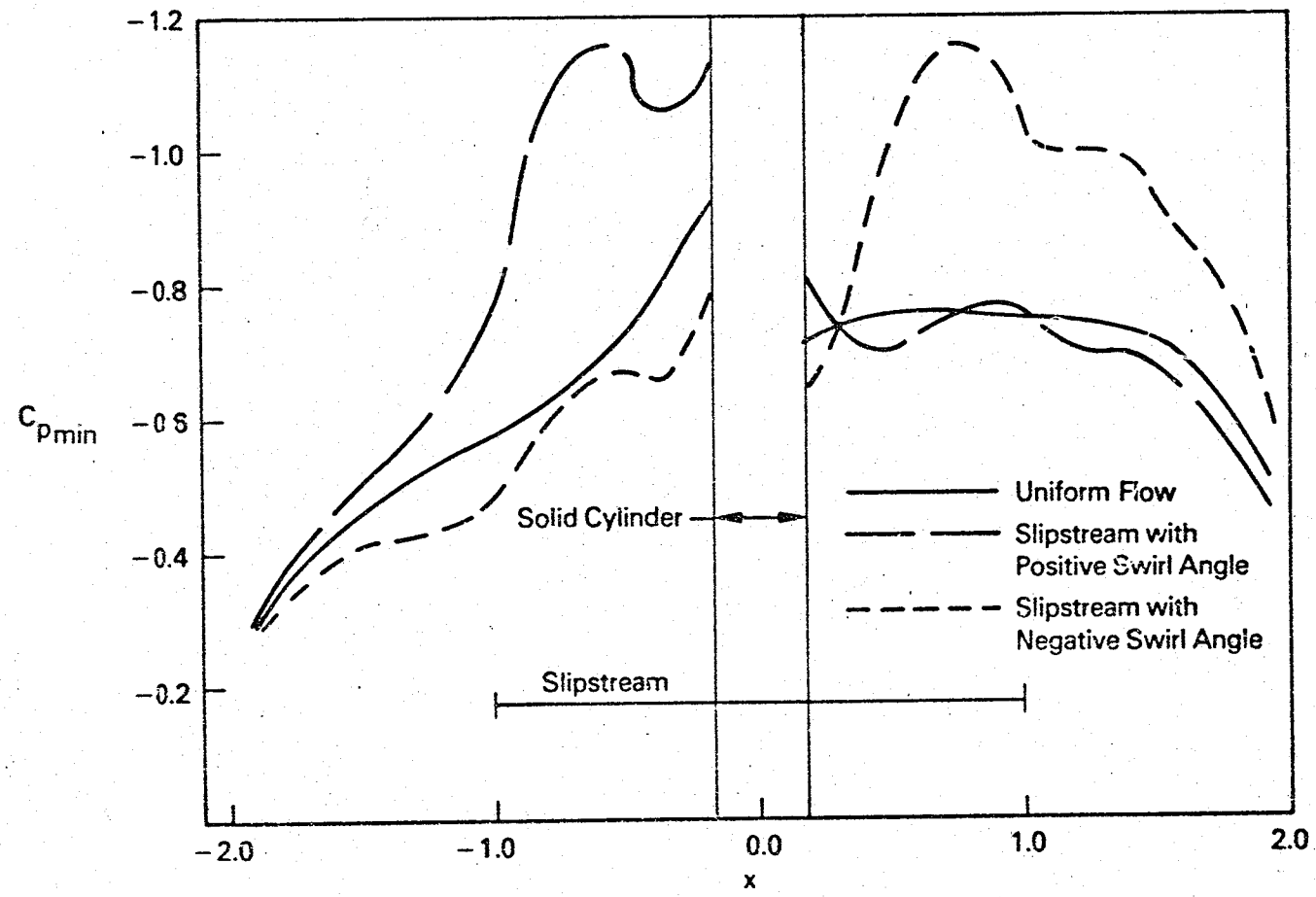

Figure 18. Minimum C_p Distribution Along Swept Wing Top.

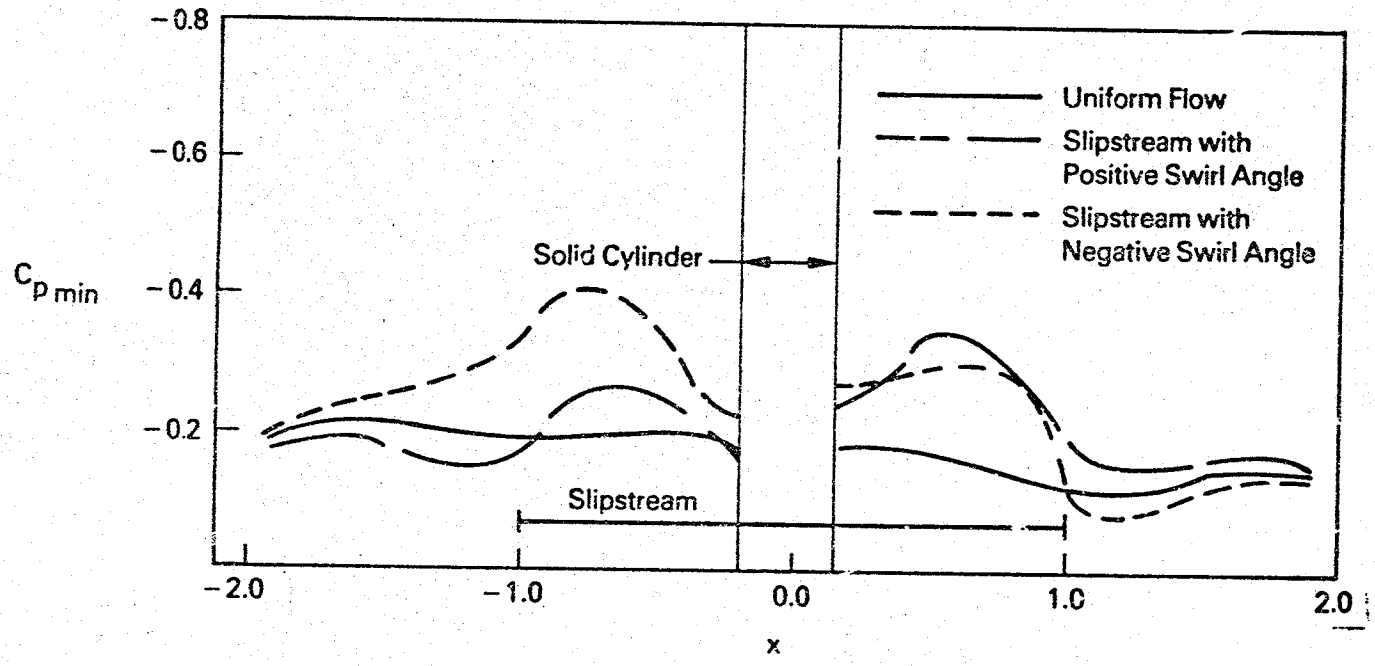

Figure 19. Minimum C_p Distribution Along Swept Wing Bottom.

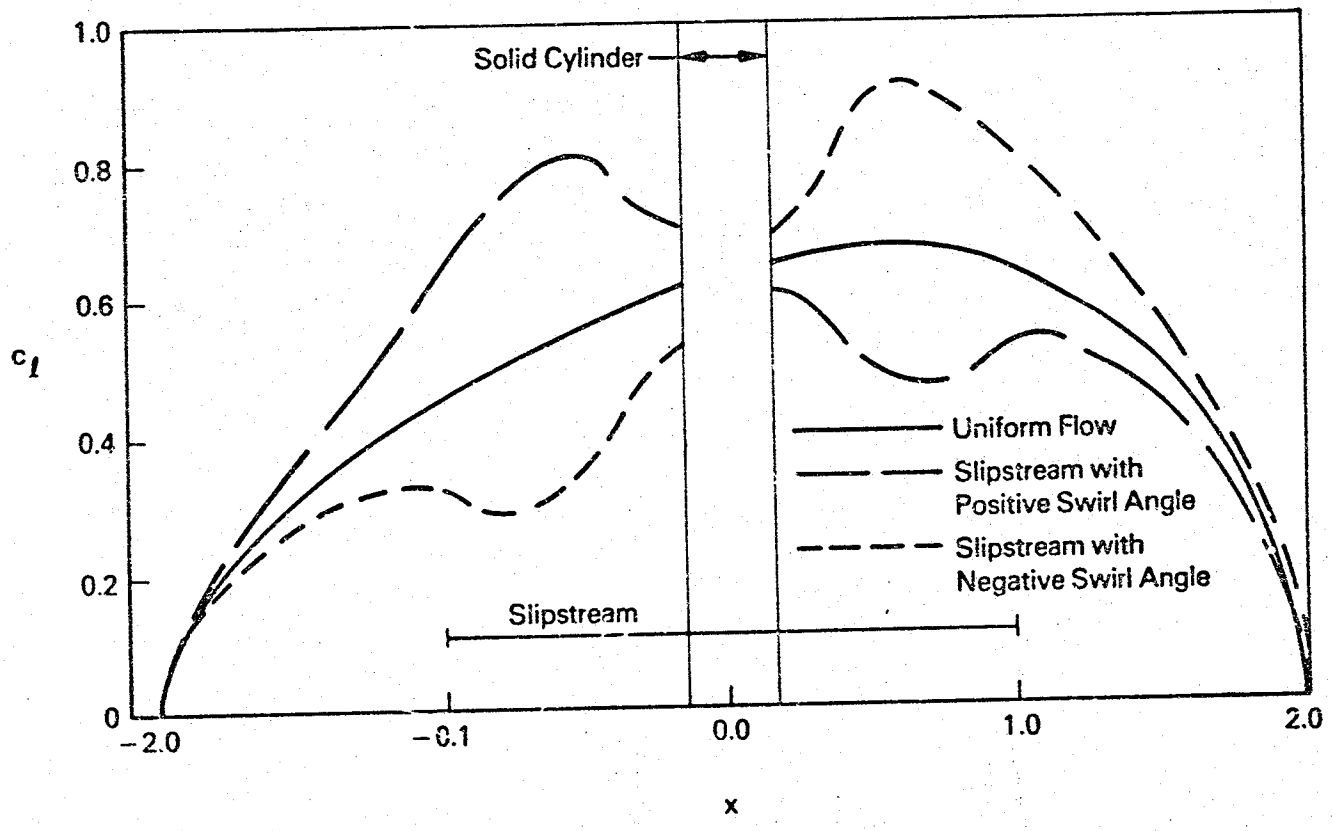

Figure 20. Lift Distribution for Swept Wing.

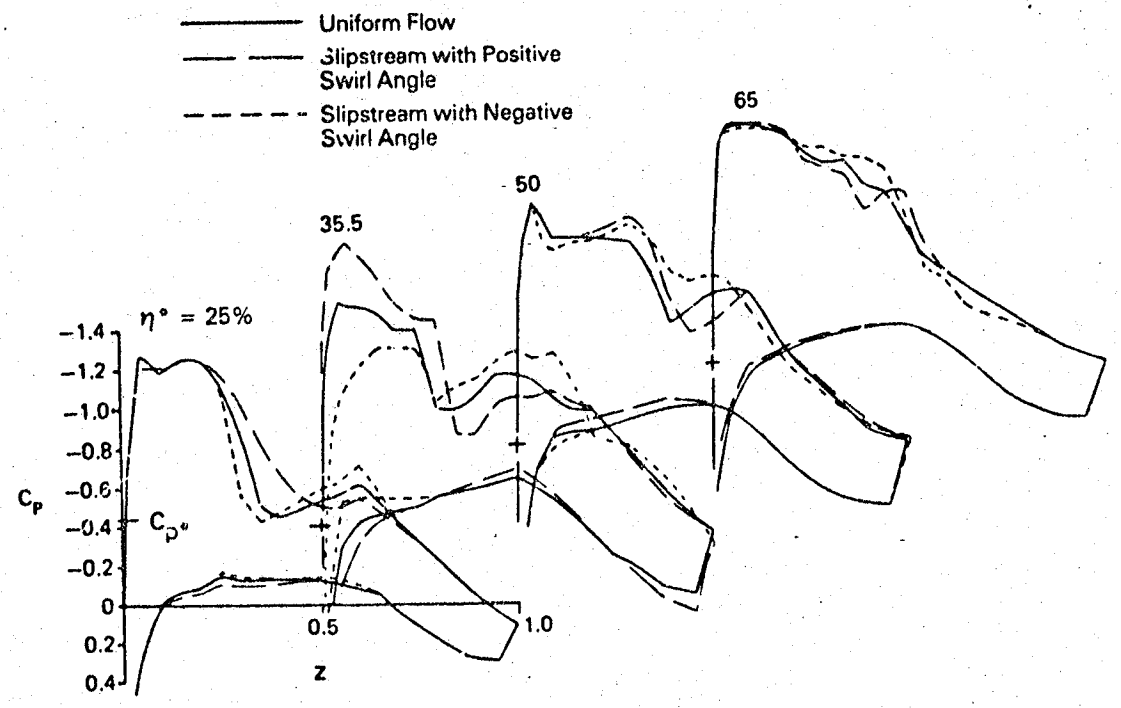

Figure 21. Wing Surface Pressure Variation Due to Power and Swirl at $M_{o\infty} = 0.8$ (Experimental Results Taken From Wedge and Crowder, 1978).

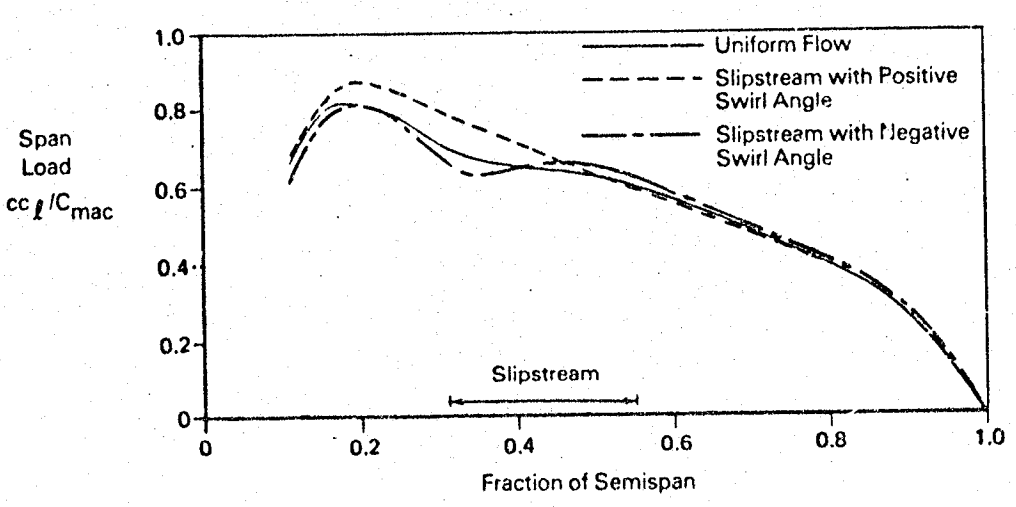

Figure 22. Span Loading at $M_{o\infty} = 0.8$ (Experimental Results Taken From Wedge and Crowder, 1978).

Appendix A

In general, the approximation of the radial velocity component at the point $(z^i, r^{j-\frac{1}{2}}, \theta^k)$ is given by

$$v^{i,j-\frac{1}{2},k} = \frac{\phi^{i,j,k} - \phi^{i,j-1,k}}{r^j - r^{j-1}} \quad .$$

This, however, is not true at mesh points for which $j = j_s$ since the slipstream boundary (across which the velocity components are discontinuous) coincides with the cylindrical surface $r = r^{j-\frac{1}{2}}$, where $j = j_s$. Expressions for the radial velocity components $v^{-i,k}$ in the inner region at the slipstream boundary and $v^{+i,k}$ in the outer region at the slipstream boundary may be found in terms of the potentials $\phi^{i,j,k}$ and $\phi^{i,j-1,k}$, where $j = j_s$, as follows:

Define a fictitious potential $\phi^{i,k}$ at the point (z^i, r^j, θ^k), where $j = j_s$, so that

$$v^{-i,k} = \frac{\phi^{i,k} - \phi^{i,j-1,k}}{r^j - r^{j-1}} \quad , j = j_s \; . \tag{A.1}$$

It follows from Equation (9) that

$$v^{+i,k} = A \frac{\phi^{i,k} - \phi^{i,j-1,k}}{r^j - r^{j-1}} \quad , j = j_s \; . \tag{A.2}$$

The axial velocity perturbation components $u^{-i-\frac{1}{2},k}$, in the inner region at the slipstream boundary, and $u^{+i-\frac{1}{2},k}$, in the outer region at the slipstream boundary, may now be expressed as follows:

$$u^{-i-\frac{1}{2},k} = \Big\{ \Big[\phi^{i,k} - \tfrac{1}{2} v^{-i,k} (r^j - r^{j-1}) \Big] - \Big[\phi^{i-1,k} - \tfrac{1}{2} v^{-i-1,k} (r^j - r^{j-1}) \Big] \Big\} / (r^j - r^{j-1})$$

$$= \frac{1}{2} \frac{1}{r^j - r^{j-1}} (\phi^{i,k} + \phi^{i,j-1,k} - \phi^{i-1,k} - \phi^{i-1,j-1,k}) \quad , j = j_s \; ,$$

and

$$u+^{i-\frac{1}{2},k} = \left\{ \left[\phi^{i,j,k} - \tfrac{1}{2}\, v+^{i,k}(r^u - r^{j-1}) \right] - \left[\phi^{i-1,j,k} - \tfrac{1}{2}\, v+^{i-1,k}(r^j - r^{j-1}) \right] \right\} / (r^j - r^{j-1})$$

$$= \frac{1}{r^j - r^{j-1}} \left(\phi^{i,j,k} - \frac{A}{2}\, \phi^{i,k} + \frac{A}{2}\, \phi^{i,j-1,k} - \phi^{i-1,j,k} + \frac{A}{2}\, \phi^{i-1,k} - \frac{A}{2}\, \phi^{i-1,j,k} \right) \quad , \; j = j_s \; .$$

Substituting the expressions for $u-^{i-\frac{1}{2},k}$ and $u+^{i-\frac{1}{2},k}$ into Equation (10), the following relation is obtained:

$$\phi^{i,k}(1 + AB) - 2B\phi^{i,j,k} + (1 - AB)\phi^{i,j-1,k} = \phi^{i-1,k}(1 + AB) - 2B\phi^{i-1,j,k} + (1 - AB)\phi^{i-1,j,k} \equiv G \quad , \; j = j_s \; . \tag{A.3}$$

This allows $\phi^{i,k}$ to be expressed as follows:

$$\phi^{i,k} = \frac{1}{1 + AB} \left(G + 2B\phi^{i,j,k} - (1 - AB)\phi^{i,j-1,k} \right) \quad , \; j = j_s \; .$$

Substituting into Equations (A.1) and (A.2), the radial velocity components become

$$v-^{i,k} = \frac{1}{(r^j - r^{j-1})\,(1 + AB)} \left(G + 2B\phi^{i,j,k} - 2\phi^{i,j-1,k} \right) \quad , \; j = j_s \; ,$$

$$v+^{i,k} = \frac{\alpha}{(r^j - r^{j-1})\,(1 + AB)} \left(G + 2B\phi^{i,j,k} - 2\phi^{i,j-1,k} \right) \quad , \; j = j_s \; .$$

Since relation (A.3) is true for all values of i, it may be applied repeatedly for decreasing values of i, obtaining

$$G = \phi^{o,k}(1 + AB) - 2B\phi^{o,j,k} + (1 - AB)\phi^{o,j-1,k} \quad , j = j_s \ .$$

Since the radial velocity component is zero at the upstream boundary, this leads to the conclusion that

$$\phi^{o,j,k} = C_o \quad , \quad j = j_s \ , j_s + 1 \ , \ . \ . \ . \ , J + 1$$

and

$$\phi^{o,k} = \phi^{o,j,k} = C_i \quad , \quad j = 1, 2, \ . \ . \ . \ , j_s - 1 \ .$$

Since

$$\phi^{o,J+1,k} = 0 \quad ,$$

it is concluded that

$$C_o = \phi^{o,j,k} = 0 \quad , j = j_s \quad ,$$

and

$$G = 2C_i \quad .$$

The constant C_i, and therefore G, may be chosen arbitrarily. Choose

$$G = 0 \ .$$

The final expressions for the radial velocity components at the slipstream boundaries are therefore

$$v_-^{i,k} = \frac{2(B\phi^{i,j,k} - \phi^{i,j-1,k})}{(r^j - r^{j-1})(1 + AB)} \quad , j = j_s \ ,$$

and

$$v_+^{i,k} = \frac{2A(B\phi^{i,j,k} - \phi^{i,j-1,k})}{(r^j - r^{j-1})(1 + AB)} \quad , j = j_s \ .$$

END

DATE

FILMED

APR 24 1981